Nano-Micro Lett. (2018) 10:69
https://doi.org/10.1007/s40820-018-0222-4

REVIEW

Nanostructured Ternary Metal Tungstate-Based Photocatalysts for Environmental Purification and Solar Water Splitting: A Review

Jun Ke[2] · M. Adnan Younis[1] · Yan Kong[1] · Hongru Zhou[2] · Jie Liu[3] · Lecheng Lei[1] · Yang Hou[1]

Received: 28 July 2018 / Accepted: 2 September 2018 / Published online: 1 October 2018

Highlights

- A series of ternary tungstate-based photocatalysts and their applications in solar energy conversion and environmental purification are systematically introduced.
- The relationship between intrinsic structures and unique properties of ternary tungstate-based photocatalysts is discussed and summarized in detail.
- Various new concepts and innovative strategies are employed to enhance the photocatalytic performance of ternary tungstate-based photocatalysts

Abstract Visible-light-responsive ternary metal tungstate (MWO_4) photocatalysts are being increasingly investigated for energy conversion and environmental purification applications owing to their striking features, including low cost, eco-friendliness, and high stability under acidic and oxidative conditions. However, rapid recombination of photoinduced electron–hole pairs and a narrow light response range to the solar spectrum lead to low photocatalytic activity of MWO_4-based materials, thus significantly hampering their wide usage in practice. To enable their widespread practical usage, significant efforts have been devoted, by developing new concepts and innovative strategies. In this review, we aim to provide an integrated overview of the fundamentals and recent progress of MWO_4-based photocatalysts. Furthermore, different strategies, including morphological control, surface modification, heteroatom doping, and heterojunction fabrication, which are employed to promote the photocatalytic

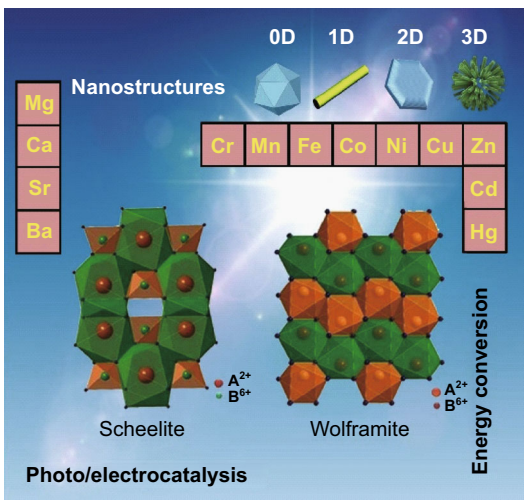

✉ Jie Liu
liujiedut@hotmail.com

✉ Yang Hou
yhou@zju.edu.cn

1 Key Laboratory of Biomass Chemical Engineering of Ministry of Education, College of Chemical and Biological Engineering, Zhejiang University, 38 Zheda Road, Hangzhou, Zhejiang, People's Republic of China

2 School of Chemistry and Environmental Engineering, Wuhan Institute of Technology, 693 Xiongchu Ave, Hongshan District, Wuhan, Hubei, People's Republic of China

3 Department of Environmental Science and Engineering, North China Electric Power University, 619 Yonghua N St, Baoding, Hebei, People's Republic of China

activities of MWO_4-based materials, are systematically summarized and discussed. Finally, existing challenges and a future perspective are also provided to shed light on the development of highly efficient MWO_4-based photocatalysts.

Keywords Ternary metal tungstates · Micro- and nanostructures · Photocatalysis · Environmental purification · Water splitting

1 Introduction

Since Fujishima and Honda in 1972 demonstrated that titanium dioxide (TiO_2) can be used as photoanode to split water excited by ultraviolet light, photocatalysis technology has been viewed as among the most promising approaches to solve the global energy crisis and environmental problems [1–3]. In general, a complete semiconductor photocatalytic cycle involves light-harvesting, photogenerated charge carrier excitation, charge separation and transfer, and surface redox reactions [4–6] that allow for the formation of reactive oxygen species (ROSs), such as free electrons (e^-), hydrogen peroxide (H_2O_2), hydroxyl (·OH), and superoxide radicals ($\cdot O_2^-$) [7, 8]. The aforementioned ROSs play crucial roles in various important applications, including photocatalysis [9–12], photoelectrocatalysis [13–17], plasma photocatalysis [18, 19], and photothermocatalysis [20–22]. Until now, TiO_2 has been among the most extensively studied semiconductor photocatalysts because of its strong oxidative ability, chemical stability, long durability, and nontoxicity [23–25]. However, the TiO_2 photocatalyst possesses a wide band gap of ~ 3.2 eV that can only absorb ultraviolet (UV) light, which is a small fraction (~ 5%) of solar light, thereby hardly harvesting the remaining solar energy [26, 27]. To efficiently utilize the majority of the solar spectrum, Fe_2O_3- [28], WO_3- [29, 30], Bi_2WO_6- [31], ZnO- [32], Bi_2O_3- [33], and NiO-based semiconductors [34] have been widely developed as photocatalysts for environmental treatment and solar water splitting (Fig. 1). Nevertheless, low sunlight utilization efficiency and quantum yield, rapid reverse reactions, and poor stability still hinder practical applications of these photocatalytic materials [35–39].

Desired photocatalysts should have a suitable band gap to achieve a high harvesting efficiency of sunlight, sufficient quantum yield, and an appropriate position of the band edge to trigger redox reactions [40–42]. For an ideal photocatalyst, the conduction band (CB) edge should be sufficiently negative to drive the photo-reduction reaction. In contrast, the valence band (VB) edge should be sufficiently positive to trigger the photo-oxidation reaction [43]. For example, in photocatalytic water splitting, when the VB edge position of the semiconductor photocatalyst is more positive than the potential of H_2O/O_2 (1.23 V vs. NHE) and the CB position is more negative than the potential of H_2/H_2O (0 V vs. NHE), the water splitting reaction can occur [44–47].

Recently, ternary tungstate-based complex oxides have been developed as potential candidates for efficient photocatalytic applications [48–50]. Tungstates are described by the general formula MWO_4 (M denotes a bivalent cation) [51] and are widely used in the luminescence, microwave ceramics, and catalytic fields, given their self-activating fluorescence effect, microwave, and optical properties [52–55]. Owing to the variety of bivalent cations, the crystal structure of MWO_4 is dependent on the size of cationic radii. According to the literature [56], MWO_4 typically has a monoclinic wolframite structure for small M^{2+} cations (M = Fe, Co, Sn, and Ni) and a tetragonal scheelite structure for large M^{2+} cations (M = Ca, Ba, Pb, and Sr), as shown in Fig. 2 [57]. During the past few decades, MWO_4 with large radii cations, including $CaWO_4$ [58, 59], $BaWO_4$ [60, 61], $PbWO_4$ [62], and $SrWO_4$ [63], has been prepared using different synthesis approaches. However, the band gaps of these MWO_4 photocatalysts are much larger than that of TiO_2 and are not suitable for practical photocatalytic applications. In contrast, the band gaps of MWO_4 with small-radii cations are considerably smaller than that of TiO_2 and could be a promising choice for the efficient utilization of solar energy [64–72]. The band-gap energies of representative MWO_4 are summarized in Fig. 3 and Table 1. In addition, the band-gap energies of various MWO_4 and the radii of the metal cations are plotted in Fig. 4. It can be seen that a flock of MWO_4 is in the yellow area, in which each MWO_4 has a smaller metal cation radius (< 0.73 Å) and narrower band-gap energy (< 3.2 eV) than those of the others. In contrast, MWO_4 with a larger cation radius have larger band-gap energy. Notably, for specific MWO_4, the band gaps presented in Table 1 are not the only ones, because the absorption light range of the semiconductors can be affected and controlled by various factors, including morphology, size, doping, and defects, thus resulting in one semiconductor material possessing several band-gap energies. By comparing the requirements of novel photocatalysts, MWO_4 with small-radius cations is more advantageous and can be further developed as highly efficient photocatalysts. In addition, it is clearly observed that ternary MWO_4 systems with a narrow band gap have transition metals as the cation component, which is earth-abundant, cost effective, and low-toxicity, benefiting wide usage in the future. However, for these visible-light-responsive pristine MWO_4, photocatalytic activities remain

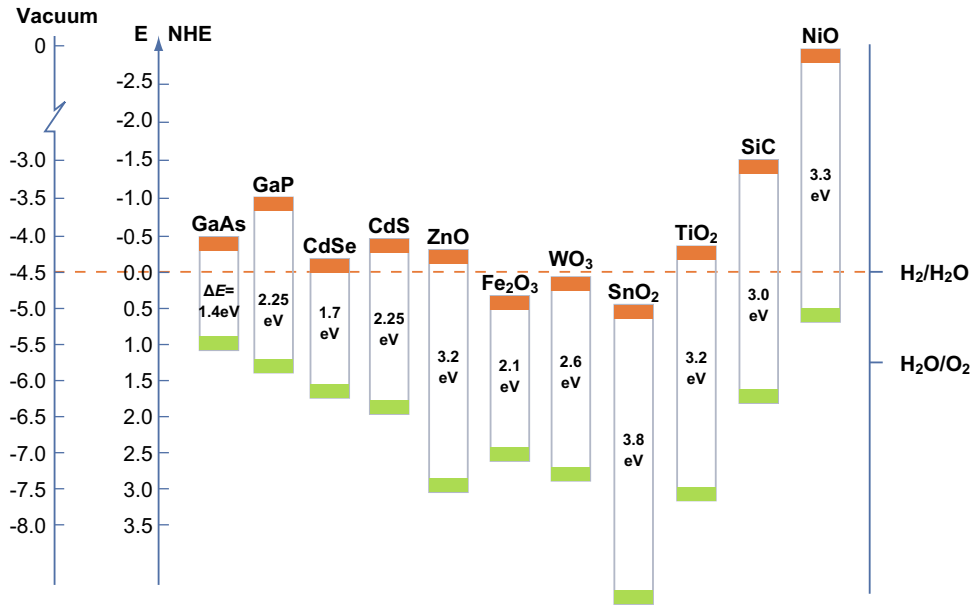

Fig. 1 Schematic overview of the band positions of representative semiconductors

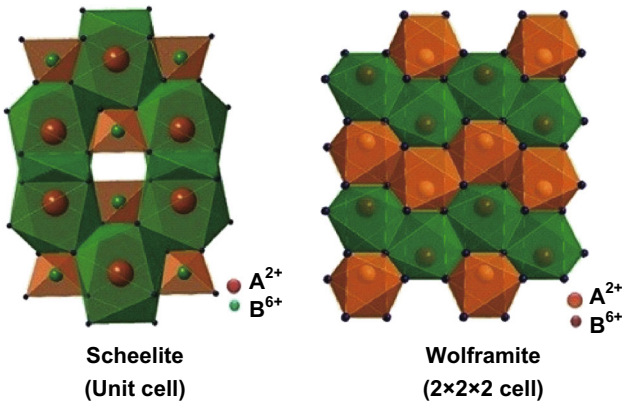

Fig. 2 Illustration of unit cells of scheelite and wolframite. Reproduced with permission from Ref. [57]. Copyright 2014 Elsevier

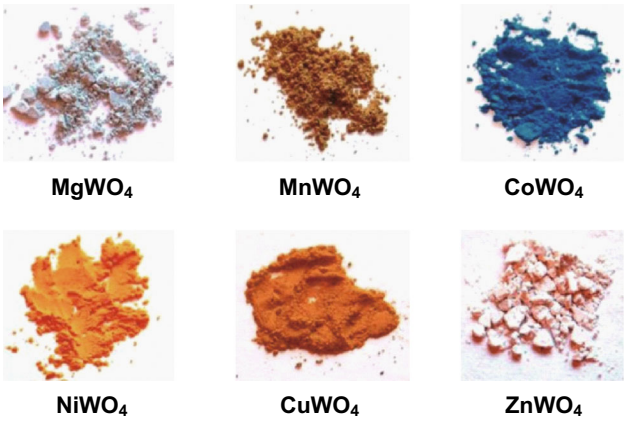

Fig. 3 Colors of different MWO_4 materials. Reproduced with permission from Ref. [51]. Copyright 2014 American Chemical Society

inadequate for practical applications because of the rapid recombination of photogenerated holes and electrons.

Herein, we provide a comprehensive review of the evolution and current state of the development and application of ternary MWO_4-based photocatalysts in environmental purification and solar water splitting. First, we discuss the fundamentals of ternary MWO_4 systems, including the crystal composition, electronic structure, and relationship between the intrinsic structures and properties. Subsequently, versatile reported strategies to improve the photocatalytic activities of pristine MWO_4 are systematically summarized. Finally, challenges and future developments of ternary MWO_4-based photocatalysts are discussed. We believe that this review provides information on recent progress in ternary MWO_4-based photocatalysts for environmental and energy applications and insight into future perspectives, which will aid the design of highly efficient semiconductor-based photocatalysts.

2 Ternary MWO_4 Photocatalysts (M = bivalent metal cations)

The photocatalytic activity of semiconductor photocatalysts is known to be closely related to their crystal and electronic structures [82]. In this section, an overview of the crystal and electronic structures of ternary MWO_4 is presented and the factors influencing their photocatalytic performance is explored.

Table 1 Band gaps, crystal sizes, and effective ionic radii of different MWO_4 materials

Compounds	Ionic radius of cation M (Å)	Band gap E_g (eV)	Crystalline sizes (nm) via Scherrer equation	References
$BaWO_4$	1.42	4.79	55	[56]
$PbWO_4$	1.29	3.2	11	[73]
$SrWO_4$	1.26	4.66	33	[56]
$CaWO_4$	1.12	4.27	32	[56]
$CdWO_4$	0.95	3.77	21	[74]
$ZnWO_4$	0.74	3.37	32	[75]
$CuWO_4$	0.73	3.2	36	[76]
$MgWO_4$	0.72	4.19	70	[77]
$SnWO_4$	0.69	2.27	36	[78]
$NiWO_4$	0.69	2.54	31	[71]
$MnWO_4$	0.66	2.97	29	[79]
$CoWO_4$	0.65	2.5	35	[80]
$FeWO_4$	0.61	2.16	50	[81]

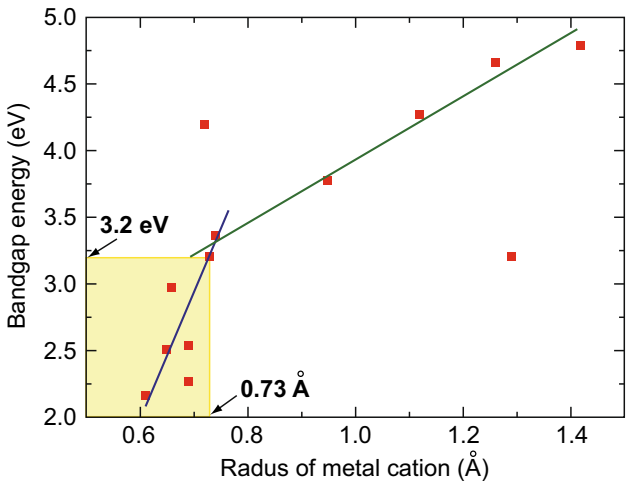

Fig. 4 Relationship between band-gap energy of MWO_4 and the radii of metal cations

2.1 Crystal Structure

As ABO_4-type compounds, ternary MWO_4 complex materials possess a typical wolframite-type monoclinic crystal structure and scheelite-type tetragonal structure. In the scheelite crystal structure, one W atom coordinates with four O atoms to form the WO_4 tetrahedral unit. In contrast, in the wolframite crystal structure, one W atom is encircled by six oxygen atoms to form the WO_6 octahedral unit. For example, Yan et al. [83] reported a tetragonal structure in $CdWO_4$ material, in which the W atom is situated in the center of the tetrahedra, forming four W–O bonds of the same bond length of 1.758 Å, with the coordination number of the Cd atom being eight. However, the monoclinic structure of $CdWO_4$ is similar to that of previously reported $MnWO_4$ [84]. Both W(VI) and Cd(II) have octahedral O coordination, in which each octahedron shares two corners with its neighbors. However, the configuration of the WO_6 octahedron leads to severe distortion in which two W–O bonds are much shorter than the other four W–O bonds. The two crystal phases of $CdWO_4$ are shown in Fig. 5. An investigation of methyl orange (MO) degradation showed that the photocatalytic performance of monoclinic $CdWO_4$ was much higher than that of tetragonal $CdWO_4$ and commercial TiO_2 under UV light irradiation, which can be ascribed to the lower lattice symmetry of the monoclinic $CdWO_4$. Furthermore, the electronic structures of the wolframite- and scheelite-type $CdWO_4$ were investigated by theoretical computations and simulations based on density functional theory (DFT). As shown in Fig. 5b-d, both monoclinic and tetragonal $CdWO_4$ are indirect-type semiconductors because the calculated bottom of the CB is not situated in the same line as the top of the VB. The calculated band gap of monoclinic $CdWO_4$ was larger than that of tetragonal $CdWO_4$, which was not consistent with the photocatalytic results. Actually, the monoclinic $CdWO_4$ consisted of distorted WO_6 octahedra, leading to the generation of dipole moments in the WO_6 octahedral units, while the tetragonal $CdWO_4$ comprised normal WO_4 tetrahedra, forming a highly symmetric lattice in the absence of dipole moments. Based on its crystal and geometric structures, the monoclinic structure of $CdWO_4$ is considered a highly efficient photocatalyst, and its catalytic performance has been extensively explored [74, 85, 86].

In addition, it has also been reported that $SnWO_4$ has two crystal structures: α-$SnWO_4$ and β-$SnWO_4$ [87]. The orthorhombic α-$SnWO_4$ is comparatively stable in the structure below 670 °C, whereas the cubic β-$SnWO_4$ is a steady structure above 670 °C. In the crystal unit of

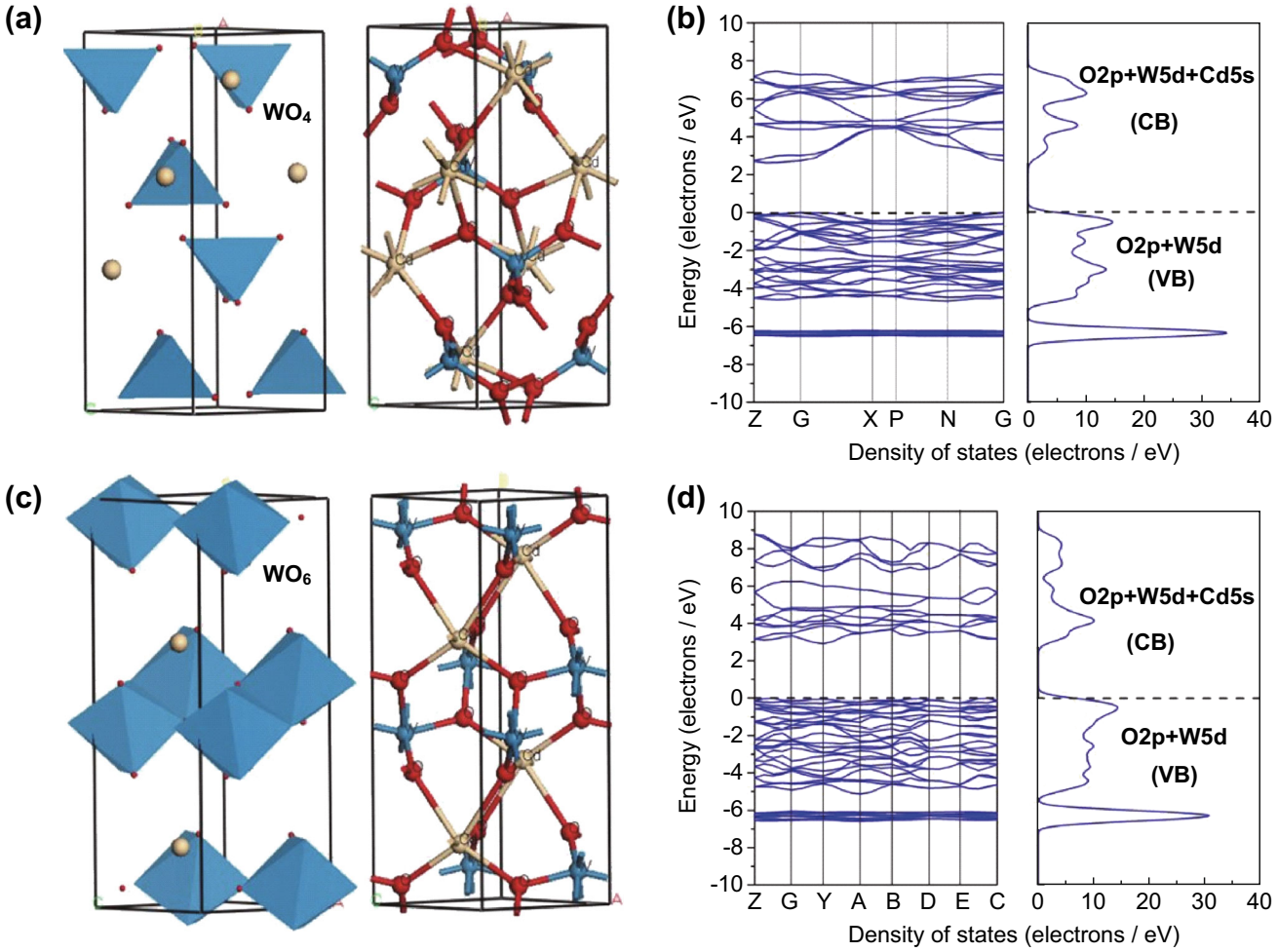

Fig. 5 Models of band structures and calculated density of states for tetragonal (**a, b**) and monoclinic (**c, d**) $CdWO_4$. Reproduced with permission from Ref. [83]. Copyright 2011 Elsevier

orthorhombic α-$SnWO_4$, a single W atom is bonded with six O atoms to constitute typical corner-shared WO_6 octahedra, while the unshared WO_4 tetrahedra are composed of a crystal unit of β-$SnWO_4$. Owing to the lone-pair effects on the Sn(II) ion, distorted SnO_6 octahedra are formed in both polymorphs. Cho et al. [88] prepared the aforementioned $SnWO_4$ materials with different types of crystal structures and investigated the relationship of the crystal structure with the optical and catalytic properties of $SnWO_4$ (Fig. 6). It was demonstrated that a difference in atom arrangement could result in an apparent difference in electronic distribution. The VB of $SnWO_4$ is constituted through high hybridization between the Sn 5 s orbital and O 2p orbital, resulting from the strong interaction between the atomic orbitals with closer energy. Meanwhile, the Sn 5 s orbitals contribute to the lower and upper energy levels of the VB, while the O 2p orbitals are dedicated to the middle energy levels of the VB. Therefore, the VB and CB electronic structures of $SnWO_4$ are totally different from those of the pristine WO_3, in which the VB and CB comprise filled O 2p orbitals and empty W 5d orbitals, respectively. The band gap of α-$SnWO_4$ was calculated to be 1.65 eV, which was lower than that of WO_3 (1.77 eV), thereby accounting for the broadening effect of the VB, which can be attributed to the contribution of the Sn 5 s orbitals. In contrast, the calculated band gap of 3.45 eV for β-$SnWO_4$ was apparently much larger than that of α-$SnWO_4$ and WO_3. Although the Sn 5 s orbitals also contribute to the VB of β-$SnWO_4$ (Fig. 6b), the increase in the band gap stems from the decreased length of the W–O bonds and enhanced crystal field splits, thus resulting in the upshifting of the CB position. Furthermore, the experimental results showed that both α-$SnWO_4$ and β-$SnWO_4$ exhibited higher photocatalytic performance for the degradation of Rhodamine B (RhB), as compared to other visible-light-response photocatalysts, such as bulk- or nanoWO_3 and nano$TiON_x$ (Fig. 6d). Moreover, the β-$SnWO_4$ showed a higher photocatalytic activity for H_2 evolution in the presence of methanol, accompanying Pt as a co-catalyst under visible-light irradiation (Fig. 6e), which

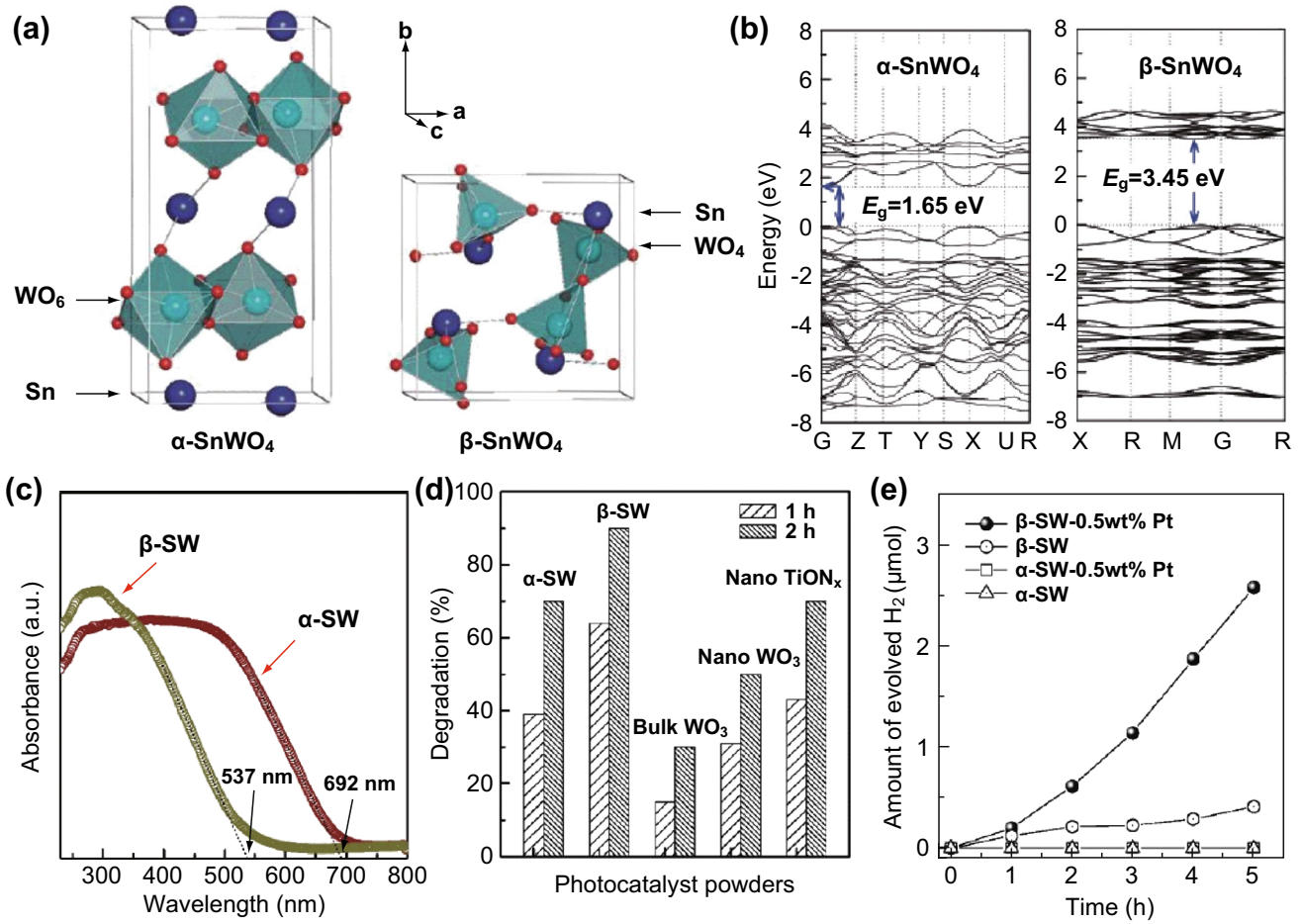

Fig. 6 **a** Crystal structures, **b** density of states, and **c** UV–Vis absorption spectra of α-$SnWO_4$ and β-$SnWO_4$. **d** Photocatalytic activity of α-$SnWO_4$ and β-$SnWO_4$ in RhB degradation. **e** H_2 evolution. Reproduced with permission from Ref. [88]. Copyright 2009 American Chemical Society

can be mainly ascribed to the higher CB edge of β-$SnWO_4$ compared to that of α-$SnWO_4$. Based on the aforementioned analysis, one can conclude that the MWO_4 photocatalysts usually possess more than two types of crystal structure, thus leading to a difference in geometries and local lattice distortions. The non-bonded electrons in the metal ion should be considered an important factor in analyzing the crystal field, particularly in an MWO_4-based asymmetric coordination environment. The distortion of the local crystal structure influences the electronic structure and band distribution, thus affecting the catalytic performances of MWO_4-based photocatalysts.

2.2 Electronic Structure

Generally, tungstates are considered derivatives of H_2WO_4 and WO_3 because of their similar elemental constitutions and crystal structures [89–91]. The DFT [92] and ab initio [93] calculations indicate that the CB of MWO_4 consists of W 5d orbitals in tungstates, as in WO_3, while the O 2p orbitals only comprise the upper part of the VB because the bivalent metal cation in tungstates contributes differently to the VB and CB positions given different outer electronic arrangements [55].

For instance, visible-light-driven $CuWO_4$ is employed for photoelectrochemical (PEC) water splitting because of its suitable band gap of 2.3 eV [94–96]. For most binary metal oxides, the VB is mainly constituted of O 2p orbitals; thus, the VB energy is usually in the range of 2.5–3.0 eV, indicating that the top of the VB is not significantly shifted in the metal oxides. For ternary metal oxides, however, the mixing atomic orbitals between the O 2p orbitals and metal orbitals could result in an apparent shift in the top position of the VB [97]. Thus, for $CuWO_4$, the VB shifts upward, in comparison to that of WO_3, accounting for the hybridization between the O 2p orbitals and Cu 3d orbitals (Fig. 7a). The upward movement in the VB position indicates a decrease in the band gap, which results in an increased visible-light absorption range [98]. However, the composition of the CB is still a topic of hot debate. DFT

calculations show that the VB of $CuWO_4$ is composed of O 2p orbitals with a small portion of Cu 3d, whereas the CB of $CuWO_4$ is composed of W 5d orbitals [99, 100]. Moreover, the Cu 3d orbitals may contribute to the CB of $CuWO_4$ except for the top of the VB [101]. Experimental results demonstrate that the CB shift of $CuWO_4$ relative to that of WO_3 can be ascribed to the incorporation of Cu 3d orbitals into the energy level of the CB [102]. Yet, strong evidence of an accurate contribution proportion of Cu 3d orbitals to the CB of $CuWO_4$ has not been obtained. Although the CB composition of $CuWO_4$ is unclear, the $CuWO_4$ photoanode presented a high photocatalytic activity with a photocurrent density of up to 0.07 mA cm^{-2} at 1.23 V and a high stability under AM 1.5G illumination (Fig. 7b, c), indicating that the $CuWO_4$ photoanode has a thermodynamic potential for water oxidation. In this system, a physical model of the photogenerated charge carrier pathways in $CuWO_4$ is proposed as shown in Fig. 7d. It shows that when the photogenerated electrons are transferred from a solution medium to a mid-gap state, the thermodynamic potential of the mid-gap state can be utilized to determine which elementary reaction is favored to occur and which is the rate-limiting reaction.

Apart from $CuWO_4$, the electronic structures of other MWO_4 materials have also been previously studied. For example, Rajagopal and co-workers [103, 104] used X-ray emission spectroscopy and DFT computation to study the electronic structures and related properties of $FeWO_4$ and $CoWO_4$ photocatalysts. The theoretical calculation results demonstrated that O 2p orbitals mainly contributed to the

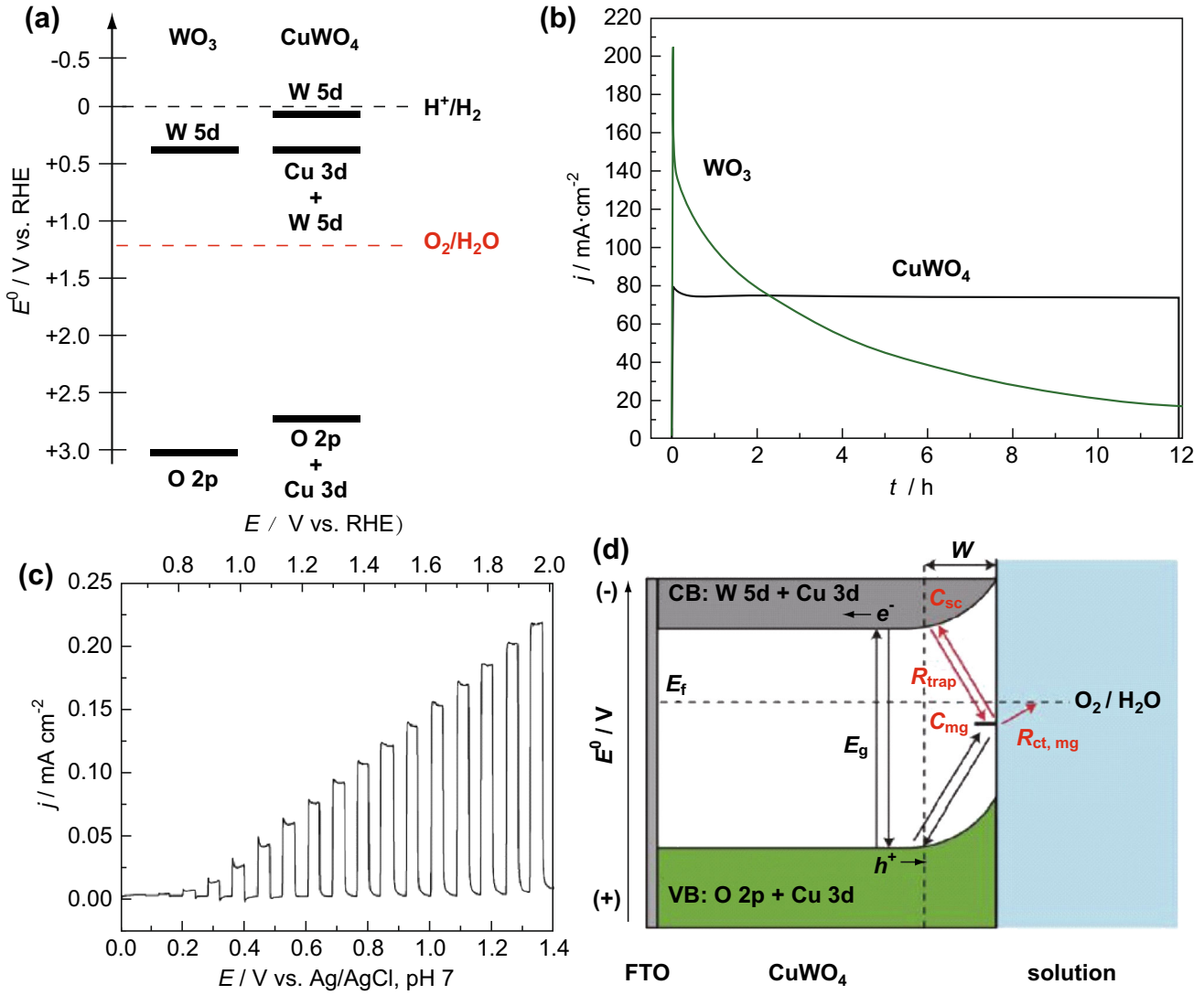

Fig. 7 **a** Distribution of energy level and **b** chronoamperometry curves of $CuWO_4$ and WO_3. **c** Polarization curve of $CuWO_4$ photoanode under AM1.5G irradiation. **d** Illustration of the physical model of charge carrier transfer in $CuWO_4$. Reproduced with permission from Ref. [102]. Copyright 2016 American Chemical Society

VB of tungstates, while the unoccupied Fe 3d orbitals and Co 3d orbitals were dominantly dedicated to the CB of $FeWO_4$ and $CoWO_4$, respectively. In addition, the density of states showed that Co 3d and W 5d orbitals also contributed to the VB regions of $CoWO_4$, similar to that of $FeWO_4$. Hence, the VBs of $FeWO_4$ and $CoWO_4$ are composed of O 2p, W 5d, and Fe/Co 3d orbitals. However, X-ray emission spectroscopy results revealed that the W 5d orbitals and O 2p orbitals are dedicated to the entire VB of the tungstates, in which the O 2p orbitals are dedicated to the upper region of the VB and W 5d orbitals are dedicated to the lower region of the VB. The theoretical results agreed well with the experimental results for $FeWO_4$ and $CoWO_4$. In addition, the electronic structure of $NiWO_4$ was obtained. For $NiWO_4$, the CB predominantly consists of W 5d orbitals and Ni 3d orbitals, while the VB primarily consists of Ni 3d orbitals and O 2p orbitals [105]. It was found that the VB composition of $NiWO_4$ is different from those of $FeWO_4$ and $CoWO_4$, which is related to the energy level distribution of the orbital electrons around the metal ions. Therefore, based on the aforementioned results, one can conclude that the electronic structures of ternary MWO_4 systems mainly depend on the position of the M^{2+} cation in the periodic table, which affects the outer electronic arrangements and hybridized electrons of the atomic orbital to the M^{2+} cation.

3 Strategies for Enhanced Photocatalytic Activity

As described in Sect. 1, ternary MWO_4 systems can act as highly promising photocatalysts for environmental purification and solar water splitting. However, among the major limiting factors in enhancing their photocatalytic activities is the rapid recombination of photogenerated electron and hole pairs. To overcome this problem and improve the overall catalytic performance of MWO_4 photocatalysts, many research groups have endeavored to develop various techniques to enhance the separation and transfer efficiency of photoexcited charge carriers inside MWO_4 or at the interface between different components. In this section, an overview of the developed strategies is provided to offer insights on their effects for the separation efficiency of photogenerated charge carriers and the corresponding catalytic performance of MWO_4-based photocatalysts.

3.1 Morphological Control

As is known, the morphology, facet exposure, and dimensions of photocatalysts have a significant influence on the photocatalytic performance. For example, nanostructured photocatalysts can exhibit excellent photocatalytic activities because the morphologies and particle sizes of the photocatalysts have a significant influence on the optical and electronic properties, which in turn affect the photocatalytic activities. For example, Yu et al. [106] prepared $FeWO_4$ samples with different morphologies, including nanoparticles, flakes, nanorods (NRs), and a mixture of NRs with flakes and tiny granules, by varying pH values during the hydrothermal process, and systematically investigated their optical properties. The results indicated that the band-gap values of $FeWO_4$ are correlated with specific morphologies. Hosseinpour-Mashkani and coworkers [75] synthesized $ZnWO_4$ nanoparticles with different sizes through a precipitation route using different polymeric surfactants. The photocatalytic degradation experiments of MO demonstrated that the $ZnWO_4$ with the smallest size of 27 nm exhibited the highest photoactivity, compared with other $ZnWO_4$ samples under UV light illumination. It has been demonstrated that particle size can affect the band gap of semiconductors because of quantum size effects. The exposed surface area of nanoparticles increases with a decrease in nanoparticle size, which can provide more active sites for a surface catalytic reaction. In addition to morphologies and particle sizes, size-related crystallinity of MWO_4 has an important influence on the photophysical and photocatalytic properties. For example, Tong et al. [74] reported nanostructured $CdWO_4$ with controllable particle sizes via a hydrothermal process and studied the effects of the particle sizes on the lattice symmetry and crystallinity. It was found that the decreased size of the $CdWO_4$ nanoparticles resulted in an expanded lattice, lowered crystallinity, and broadened band gap. Meanwhile, the decrease in particle sizes caused an apparent decrease in the photocatalytic activity of $CdWO_4$. These results illustrate that size-related properties are closely correlated with the photocatalytic activity of MWO_4. Apart from the effects of the aforementioned factors on photoactivity, the crystal phase of MWO_4 is also regulated by various synthetic routes to obtain the desired physiochemical and optical properties, because different crystal phases can lead to distinct differences in the exposure of crystal facets and reactivities. For instant, different crystal phases of $CdWO_4$ nanocrystals were prepared by adjusting the used solvents for photocatalytic H_2 evolution (Fig. 8) [86]. The solvent significantly affected the chelation and growth of the $CdWO_4$ material, thus leading to apparent differences in the crystal phase. m-$CdWO_4$ nanocrystals with particle sizes ranging from 4.4 to 31 nm can be prepared using short-chain solvents, while t-$CdWO_4$ nanocrystals can be easily prepared utilizing long-chain solvents. The obtained m-$CdWO_4$ nanocrystals exhibited much higher H_2 production than the t-$CdWO_4$ nanocrystals.

During recent years, the construction of hierarchical structures to tune the morphologies of MWO_4

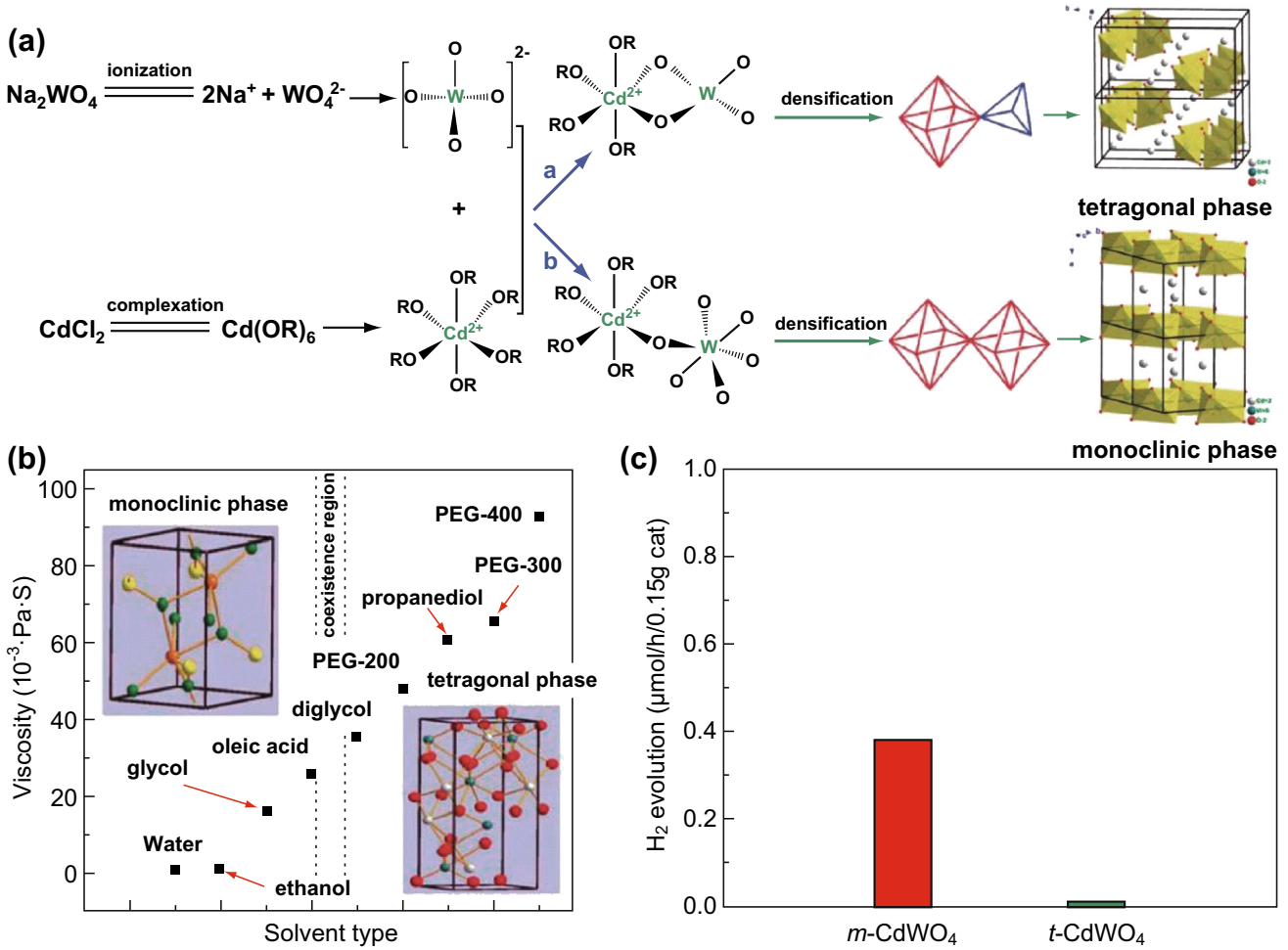

Fig. 8 **a** Formation mechanism of m-$CdWO_4$ and t-$CdWO_4$ and the **b** relationship between different crystal phases of $CdWO_4$ and used solvents. **c** Photocatalytic H_2 evolution of m-$CdWO_4$ and t-$CdWO_4$ under visible light irradiation. Reproduced with permission from Ref. [86]. Copyright 2012 Royal Society of Chemistry

photocatalysts has attracted more attention, because hierarchical structures can offer more exposed surfaces and/or active sites. For example, highly efficient hydrophobic $CdWO_4$ microspheres were synthesized by Hou et al. [107] through a microwave-assisted interfacial hydrothermal strategy. The $CdWO_4$ microspheres showed enhanced photocatalytic activity for the degradation of MO under mercury lamp irradiation (Fig. 9). The advantages of a hierarchical structure for the enhanced photocatalytic activity of MWO_4 are supported by several research groups [108–111]. Chen et al. [112] prepared $FeWO_4$ microspheres by using an ethylene glycol-assisted solvothermal approach, in which ionic1-octyl-3-methylimidazolium tetrachloroferrate was used as one of the starting materials and played an important role as both a reactant and template. The microsphere-like $FeWO_4$ material consisted of numerous nanosheets and exhibited a much better photo-Fenton activity in water purification (Fig. 10) because of the generation of hydroxyl radicals, which are produced from the chemical reaction between Fe^{2+} on the surface of $FeWO_4$ and H_2O_2. The formed Fe^{3+} was further reduced by the photoinduced electrons to generate Fe^{2+}, which is a virtuous cycle, to maintain high photocatalytic performance. Recently, Zhou et al. [113] synthesized an urchin-like $MnWO_4$ hierarchical structure through a facile hydrothermal process with the assistance of cetyltrimethylammonium bromide (CTAB) as surfactant. The introduction of CTAB as the surfactant had significant effects on the morphology and magnetic properties of the $MnWO_4$ nanocrystals. Subsequently, Xing et al. [114] provided a new route for the synthesis of a complex three-dimensional (3D) $MnWO_4$ nanostructure. In this case, a 3D flower-like $MnWO_4$ nanocomposite was synthesized using a microemulsion-based solvothermal approach. Moreover, Chen et al. [115] discussed the effect of the morphology of β-$SnWO_4$ on its photocatalytic performance, in which the β-$SnWO_4$ with a multi-armed architecture and hexahedral symmetry displayed much higher photocatalytic activities

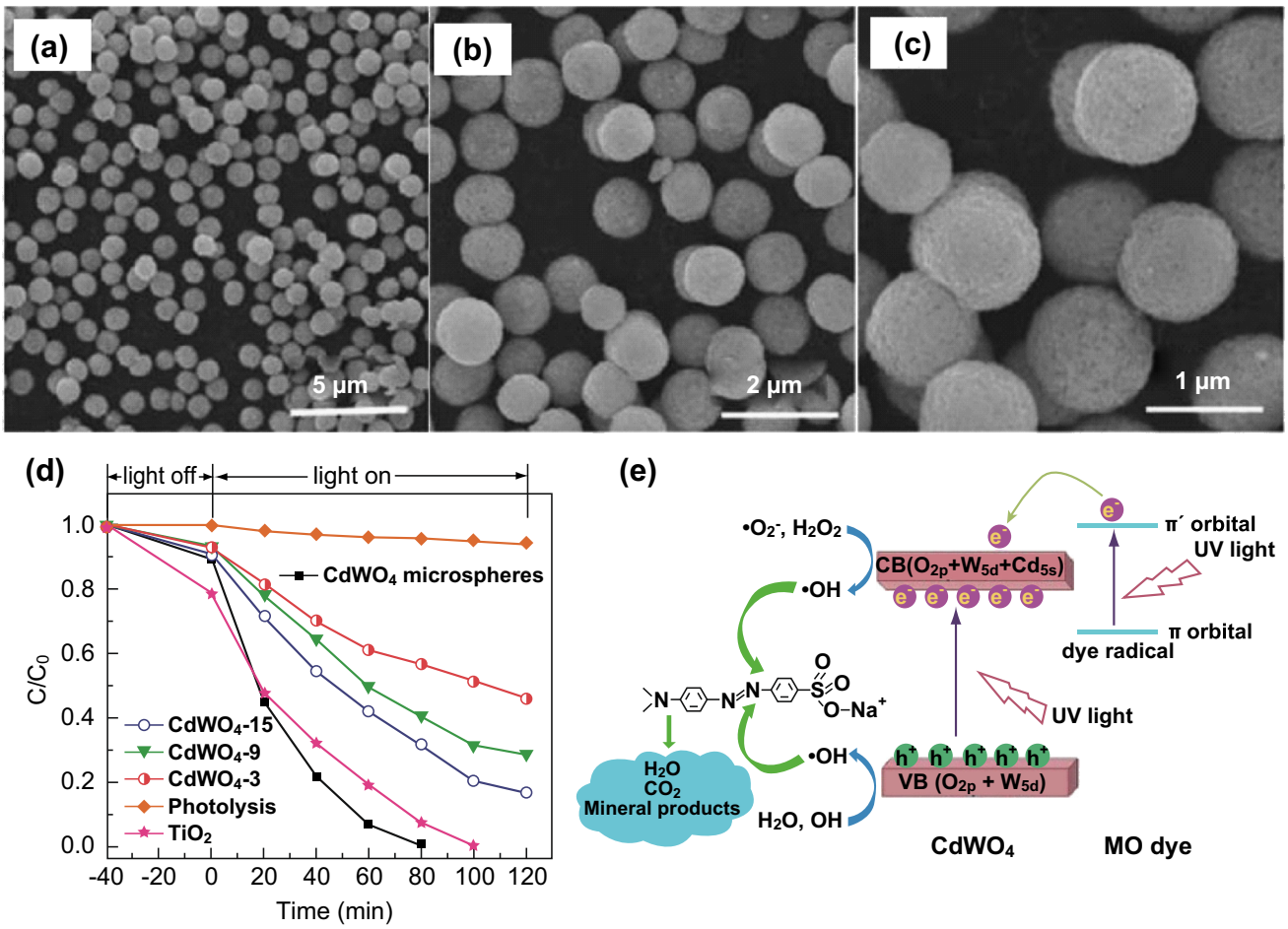

Fig. 9 **a–c** FESEM images of $CdWO_4$ microspheres. **d** Photocatalytic degradation efficiencies of MO in the presence of different photocatalysts. **e** Photocatalytic mechanism for $CdWO_4$ microspheres. Reproduced with permission from Ref. [107]. Copyright 2014 Royal Society of Chemistry

than those of both cubic β-$SnWO_4$ and commercial WO_3. Hence, more surface reaction sites induced by the hierarchically multi-armed architecture and the band structure reframing caused by incorporation of the Sn atom into WO_3 contributed to the excellent photocatalytic activity.

Previously, crystal facet exposure was viewed as an effective strategy to regulate the surface physicochemical and photophysical properties, thus optimizing the reactivity and selectivity of photocatalysts. In general, a crystal facet with a high percentage of unbonded atoms has superior reactivity in comparison to that with a low ratio of unpaired atoms. In addition, crystal facets possessing high surface energy are usually unstable during preparation. It is desirable to synthesize photocatalysts with a high exposure of high-energy crystal facets to enhance the photocatalytic reactivity and selectivity. Using DFT calculations, Qiu and co-workers [116] reported the atom distributions and electronic properties of $MnWO_4$ and $FeWO_4$ with specific facets. The calculated results showed that the {010} and {100} facets have the lowest surface energies in wolframite-type $FeWO_4$ and $MnWO_4$, respectively. Meanwhile, it was observed that the Fe and Mn atoms on the {010} and {001} planes as absorption sites can be used to absorb anions. These results indicated that the exposed {100} facet in $MnWO_4$ and $FeWO_4$ can provide a path for improving their photoactivities, while the other exposed facets can offer a certain selectivity to a specific reaction, such as a dichlorination reaction. Recently, Ungelenk et al. [117] synthesized phase-pure β-$SnWO_4$ with truncated rhombic dodecahedrons using a microemulsion technique with CTAB as a co-surfactant with n-hexanol (Fig. 11). Benefitting from the rapid Na_2WO_4-induced nucleation and slow crystal growth controlled by the CTAB-mediated microemulsion reaction, the as-prepared β-$SnWO_4$ with truncated rhombic dodecahedrons was encircled with highly exposed {100} and {110} facets. By comparing a series of β-$SnWO_4$ to other photocatalysts of Ag_3PO_4 and m-$BiVO_4$, the β-$SnWO_4$ microcrystals with exposed {100} and {110} facets showed outstanding photocatalytic activity for the degradation of organic pollutants under

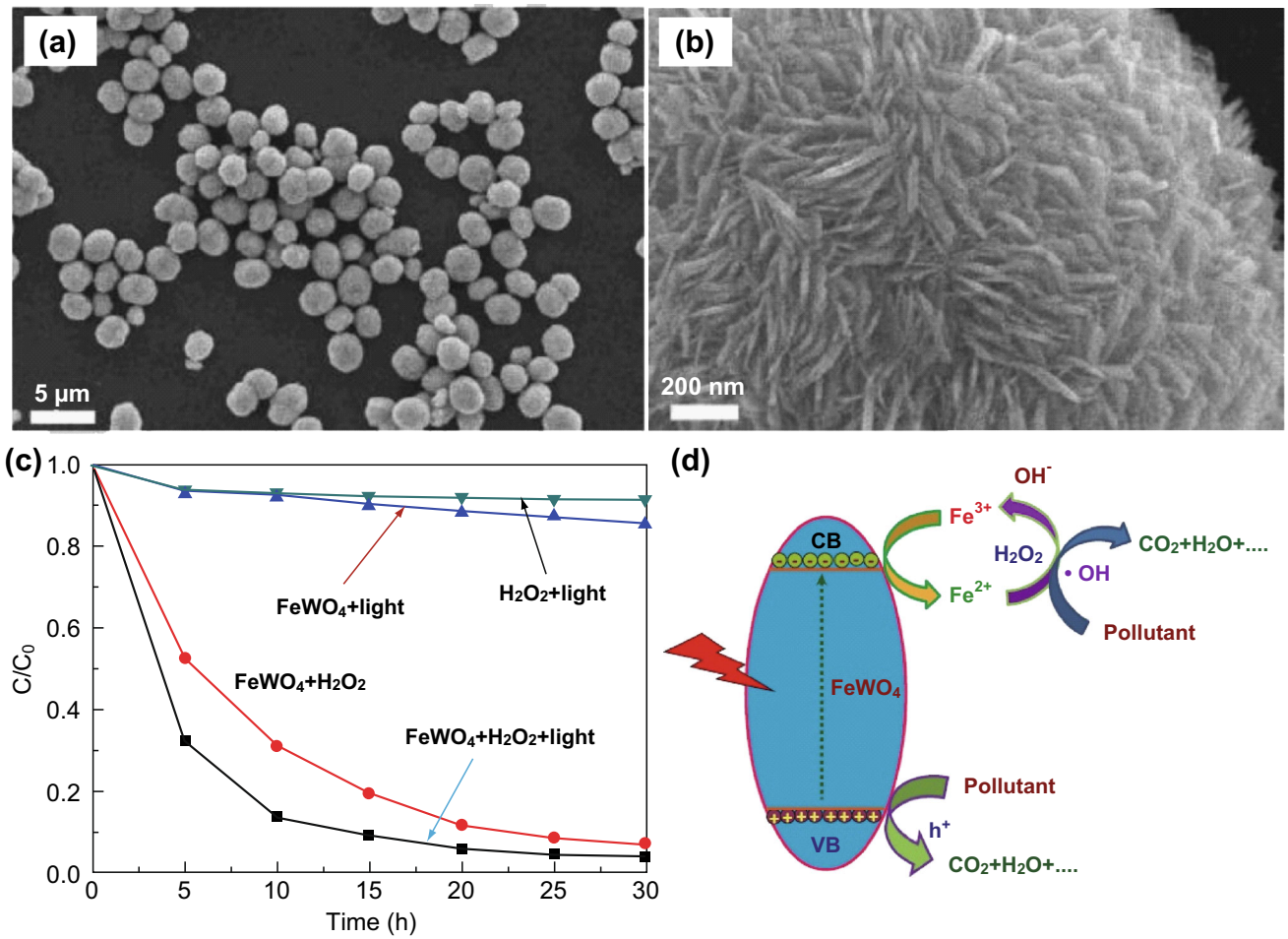

Fig. 10 **a**, **b** FESEM images of $FeWO_4$ microspheres. **c** Photocatalytic performance of $FeWO_4$ microspheres for the degradation of RhB. **d** Schematic illustration of photocatalysis mechanism for $FeWO_4$ microspheres. Reproduced with permission from Ref. [112]. Copyright 2016 Elsevier

daylight irradiation, which was far better than that of other photocatalysts, including bulk non-faceted β-$SnWO_4$ and spherical-like β-$SnWO_4$ nanoparticles. In addition, given the slight difference in specific surface area between the faceted β-$SnWO_4$ and non-faceted β-$SnWO_4$, it was concluded that optimized facet exposure was the predominant reason for the distinct photocatalytic activity. In addition, Tian et al. [118] reported a facile solvothermal method for the synthesis of hierarchical $FeWO_4$ nanosheets with an exposed {100} facet, which exhibited excellent peroxidase-like catalytic activity for oxidizing the peroxidase substrate of 3,3′,5,5′-tetramethylbenzidine (TMB) because of the formation of hydroxyl radicals in the presence of H_2O_2. The surface Fe^{2+} in $FeWO_4$ can activate the H_2O_2 molecule to produce active hydroxyl radicals for the oxidation of TMB. The results clearly indicated that the {100} facet of $FeWO_4$ had a much higher ratio of Fe atoms than that of the {001} and {010} facets, which explained the enhanced catalytic activity of $FeWO_4$ with the exposed {100} facet.

Owing to the high surface area and large absorption cross section it provides, a low-dimensional nanostructure can be constructed to manipulate and regulate optical, electrical, and magnetic properties [119, 120]. Low-dimensional nanostructures including those that are one-dimensional (1D) or two-dimensional (2D) cause the growth of a crystal along one or two directions, which can contribute to more exposure of specific surface facets. For example, 1D $CdWO_4$ NRs were prepared using microwave or hydrothermal approaches and exhibited excellent photocatalytic activity for environmental treatments, as compared to nanoparticles [121–123]. Kovacs and co-workers [111] prepared a series of $FeWO_4$ with different morphologies, including nanoparticles, NRs, and nanosheets, by varying the Fe precursors. The nanosheet-like $FeWO_4$ with band-gap energy of ~ 2.2 eV exhibited excellent absorption ability throughout the UV and visible-light range, which was attributed to the formation of a cavity assembled by nanosheets that resulted in enhanced photon harvest. Therefore, the $FeWO_4$ nanosheets showed higher

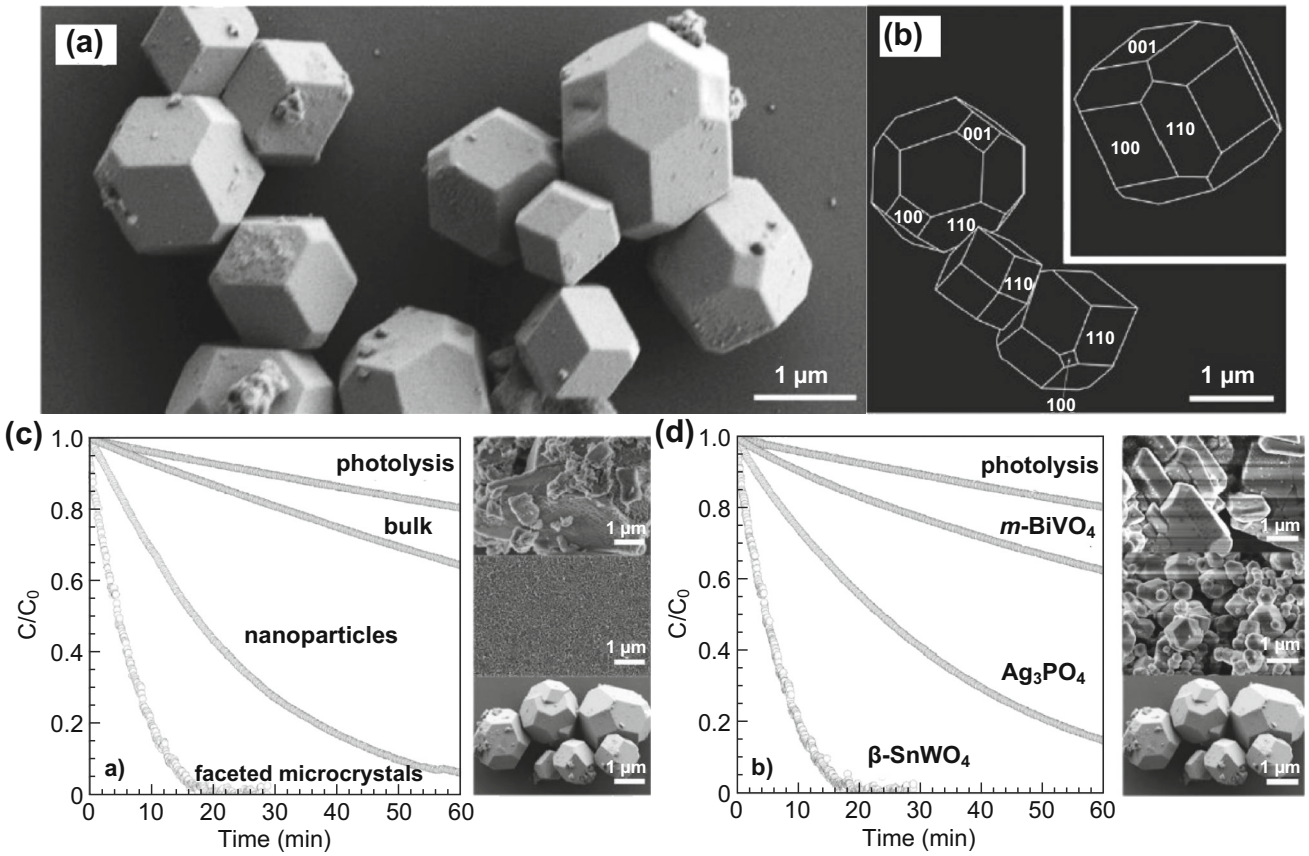

Fig. 11 **a**, **b** FESEM images of faceted β-$SnWO_4$ microcrystals. **c, d** FESEM images and photocatalytic activities for the degradation of MB over faceted β-$SnWO_4$ microcrystals, bulk β-$SnWO_4$, and β-$SnWO_4$ nanoparticles under sunlight irradiation. Reproduced with permission from Ref. [117]. Copyright 2012 Royal Society of Chemistry

photocatalytic activity than other control samples for the degradation of organic dyes under visible-light irradiation.

3.2 Surface Modification

Considering that the photocatalytic reaction proceeds on the surface of semiconductors, the surface physiochemical properties of semiconductor-based photocatalysts are important for improvement of photocatalytic activity. Several strategies, including chemical etching, surface coverage, and co-catalyst attachment, have been developed to tune the surface properties of semiconductor-based photocatalysts.

The purpose of etching techniques, such as chemical etching and laser or electron-beam irradiation, is to form non-stoichiometric or metal/oxygen vacancies on the surface of an inorganic semiconductor. The formation of metal or oxygen vacancies has proven to have an apparent influence on the electronic distribution because of the introduction of a new defect energy level, thus affecting the light absorption range and photocatalytic activity. For example, Aloysius-Sabu et al. [124] investigated the effects of intentional electron-beam irradiation on the crystal phase, size, and surface properties of $CaWO_4$ that was prepared through chemical precipitation and heat treatment. The experimental results showed that the high-energy electron beam significantly affected the crystal size and surface structure, but not the crystal phase. When the $CaWO_4$ photocatalyst was irradiated by an electron beam, the surface atomic layers of $CaWO_4$ underwent stretching and compressive strain, which resulted in the formation of surface defects and a new energy level in the band gap. Therefore, an apparent absorption tail and narrowed band-gap energy were observed in the irradiated $CaWO_4$ sample. In addition, Lin et al. [125] prepared a visible-light-driven Ag_2WO_4 photocatalyst through a laser irradiation route in liquid using commercial Ag_2WO_4 as a starting material for organics degradation and H_2 evolution. Because of the laser irradiation, the crystal structure was recrystallized and a lattice defect was introduced in Ag_2WO_4, leading to the formation of intermediate energy levels with a decrease of 0.44 eV in the band gap. The synthesized Ag_2WO_4 exhibited a photocatalytic H_2 evolution rate as high as 13.73 μmol $(hg)^{-1}$ under visible-light illumination, while no H_2 evolution was observed in the unirradiated

commercial Ag_2WO_4 sample, which was ascribed to a large band gap of 3.22 eV for bulk Ag_2WO_4.

However, to enhance the solar conversion efficiency of tungstates, surface coverage has been adopted to increase the charge transfer efficiency by means of passivating the surface via deposition of a protective layer. For example, Karthiga and co-workers [71] reported the synthesis of $NiWO_4$ nanoparticles modified by a plant extract, *A. indica*, as a capping agent through a precipitation route for enhanced photocatalytic activity. The introduction of *A. indica,* which possesses rich water-soluble heterocyclic groups, led to the formation of a passivation layer on the surface of the $NiWO_4$ nanoparticles, which allowed the $NiWO_4$ nanoparticles to separate well from each other. In comparison to the bare $NiWO_4$ nanoparticles, the *A. indica*-coated $NiWO_4$ exhibited a much higher photocatalytic activity for the degradation of organic contaminants under visible-light irradiation because of the formation of the passivation layer of the plant extract, which significantly suppressed the recombination of photoinduced electrons and holes. Meanwhile, modified $NiWO_4$ presented higher antimicrobial activity as compared with pure $NiWO_4$ nanoparticles.

Apart from chemical etching and surface coverage strategies, attachment of noble metal co-catalysts (such as, Pt, Au, and Ag) is another effective means to tune the surface photophysical properties of photocatalysts because of the surface plasmon resonance (SPR) effect [126, 127]. The SPR effect not only significantly enhances visible-light absorption, but also produces a localized electromagnetic field, thus improving the separation efficiency of the photogenerated charge carriers at the interfaces between the metal and semiconductor [128, 129]. Furthermore, the metal–semiconductor heterostructure could efficiently suppress the recombination of photogenerated electrons and holes because of the formation of Schottky barriers at the contacted interface, thus enhancing photocatalytic performance [126]. Based on the aforementioned features, the introduction of a noble metal into MWO_4 is a feasible approach to realize enhancement of its photocatalytic performance. Recently, Liu et al. [130] prepared Ag nanoparticles (NPs)/α-$SnWO_4$ nanosheets through microwave-assisted anchoring of Ag NPs on $SnWO_4$ nanosheets. The loading amount of the deposited Ag NPs was well-tuned by adjusting the initial concentration of the Ag^+ precursor and CTAB surfactant (Fig. 12a). The obtained Ag NPs/α-$SnWO_4$ hybrid showed enhanced light absorption ability and photocatalytic activity for the degradation of MO, compared to pure α-$SnWO_4$, under visible-light irradiation. Moreover, the hybridized Ag NPs/α-$SnWO_4$ system exhibited improved transient photocurrent density in comparison to that of pristine α-$SnWO_4$ (Fig. 12c), indicating that more photoinduced charge carriers could be produced and further participated in the redox reaction. In addition, Yan et al. [131] synthesized Ag-loaded $CdWO_4$ NRs using a photo-assisted co-precipitation method with the addition of the PEG-100 surfactant, which exhibited a higher photocatalytic activity than that of pure $CdWO_4$ NRs because of the SPR effect. In another study, Au NPs were utilized to construct Schottky barriers in an MWO_4-based system. For instance, Au NRs/$MnWO_4$, with a diameter of 20-40 nm, was reported by Chakraborty et al. [132] to enhance the photocatalytic decomposition of 2-propanol and phenol. The Au NPs as co-catalysts in the Au/$MnWO_4$ hybrid were beneficial to multi-electron O_2 reduction and hole oxidation.

3.3 Heteroatom Doping

It has been demonstrated that the introduction of impurities via doping of heteroatoms into a semiconductor can influence the photocatalytic performance [133, 134]. However, heteroatom doping might either have positive or negative impacts for the photocatalytic performance of semiconductors, because there are two different doping levels—the shallow level near the surface and deep level inside the body [135]. Deep-level doping can usually provide a recombination center to intensify the meaningless dissipation of absorbed photons, thus undermining the photocatalytic activity. Therefore, appropriate heteroatom doping is vital to increasing the photocatalytic performance of heteroatom-doped photocatalysts. To overcome shortcomings, such as a narrow wavelength range and rapid recombination of photogenerated electron–hole pairs, a few recent reported types of heteroatom doping to enhance the photocatalytic performances of ternary MWO_4 materials are reviewed and their roles discussed in detail.

In heteroatom doping, the dopants are mainly non-metal elements such as B [136], Cl [137], and various transition metals (Zn, Ni, Fe, Co, etc.) [138, 139], which exhibit enhanced photocatalytic activity for mineralizing organic pollutants. For instance, Chen et al. [140] synthesized F-doped $ZnWO_4$ nanocrystals (F_i-$ZnWO_4$ nanocrystals) using a two-step hydrothermal process and investigated its chemical bonds via band structure calculations (Fig. 13). In comparison to undoped $ZnWO_4$, the F_i-$ZnWO_4$ nanocrystals exhibited significant red shifts and improved light absorption in the range of UV–visible light, which resulted in enhancement of photocatalytic activity for the degradation of RhB under mercury lamp irradiation. Additionally, the experimental results showed that the crystallinity and morphology of the prepared F_i-$ZnWO_4$ was strongly related to the photocatalytic activity. F_i-$ZnWO_4$ exhibited higher photocatalytic performance for the degradation of organic dyes than F_i-$ZnWO_4$ NPs. Based on the theoretical calculation results, the enhancement of the photocatalytic

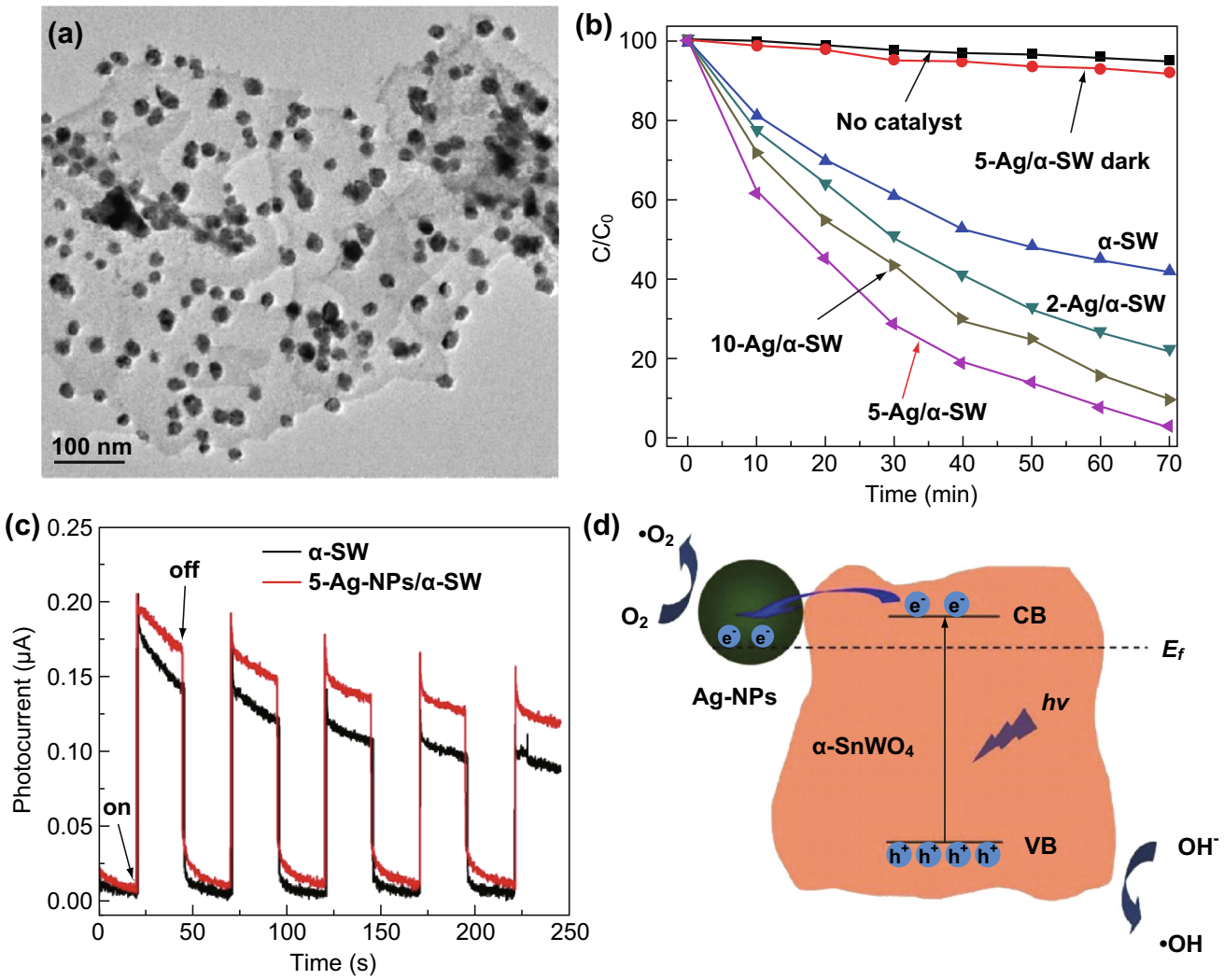

Fig. 12 **a** TEM image and **b** photodegradation efficiency of Ag NPs/α-$SnWO_4$ under visible-light irradiation. **c** Transient photocurrent response for different samples. **d** Illustration of photocatalytic mechanism of Ag NPs/α-$SnWO_4$. Reproduced with permission from Ref. [130]. Copyright 2017 Elsevier

activity of F_i-$ZnWO_4$ might be ascribed to the following reasons. First, F-doping increased the absorptivity of F_i-$ZnWO_4$, such that it could absorb more reactants to enhance the photocatalytic activity. Second, a new half-filled state was introduced into the original band gap of $ZnWO_4$ accompanying the F-doping, which could provide more holes to enhance the photocurrent density of F_i-$ZnWO_4$. Thus, heteroatom doping could efficiently improve the photocatalytic activities of MWO_4 by introducing a new energy level to regulate the original electronic structure.

Apart from the introduction of non-metal elements, transition metal elements can also be a potential dopant. For example, Su et al. [141] prepared Zn^{2+}-doped $SnWO_4$ nanocrystals, and reported that the morphological alteration of $SnWO_4$ nanocrystals from nanosheets to nanowires can be controlled by Zn^{2+} doping. Consequently, the Zn^{2+}-doped $SnWO_4$ exhibited a greater Brunauer–Emmett–Teller surface area (54 and 100 $m^2\ g^{-1}$ for pure $SnWO_4$ and Zn^{2+}-doped $SnWO_4$, respectively), narrowed band gap (2.68 and 2.64 eV for pure $SnWO_4$ and Zn^{2+}-doped $SnWO_4$, respectively), and highly enhanced photocatalytic performance for the degradation of MO (95% and 30% for pure $SnWO_4$ and Zn^{2+}-doped $SnWO_4$, respectively) compared to that of pure $SnWO_4$. In addition, Song et al. [142] reported the synthesis of Zn-doped $CdWO_4$ NRs using a hydrothermal process to enhance the photocatalytic conversion efficiency of organic pollutants into low-toxicity small molecules under simulated sunlight irradiation. The influence of the Zn-doping amounts on the crystal phase, morphology, and optoelectronic properties of $CdWO_4$ NRs was also systematically investigated. Compared to the undoped sample, the Zn-doped $CdWO_4$ NRs exhibited much higher photocatalytic activity, which was assigned to

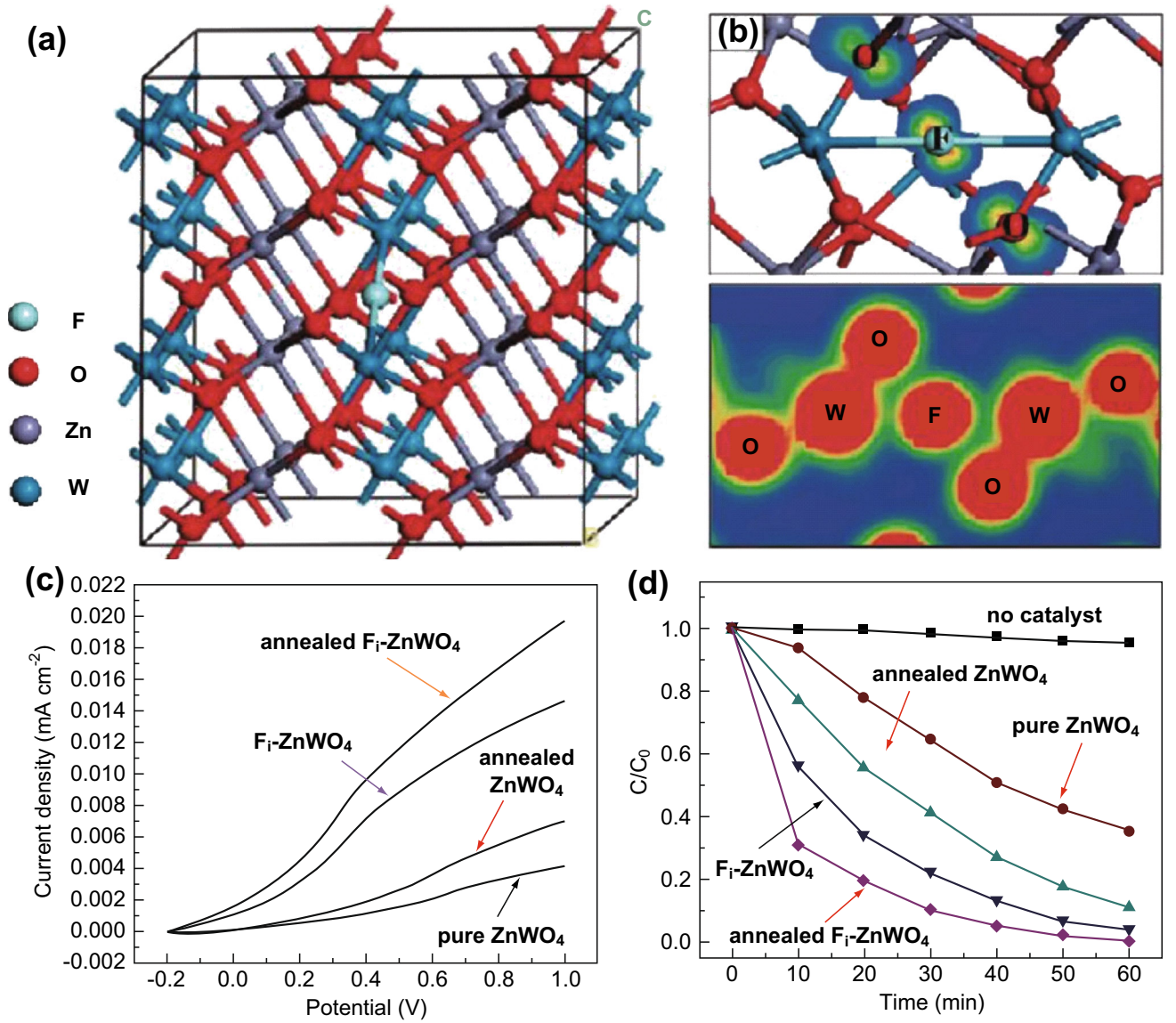

Fig. 13 **a** Geometric structures for the F_i-$ZnWO_4$. Spin density (top) and total charge density (bottom) for F_i-$ZnWO_4$. **c** Photocurrent density of the synthesized samples under UV-light irradiation. Photocatalytic degradation of RhB over different samples under UV light irradiation. Reprinted with permission from Ref. [140]. Copyright 2010 American Chemical Society

the narrowed band gap due to Zn-doping. Heteroatom doping could be an effective means to tune the distribution of the energy level and further enhance the photocatalytic performance of MWO_4 without consuming excess foreign substances.

Recently, rare earth element-doped photocatalysts have attracted more attention because of their special 4f electron configuration, which could be beneficial for introducing a suitable energy level into the original band gap of MWO_4 [143]. Phuruangrat et al. [144] synthesized Ce-doped $ZnWO_4$ using a hydrothermal process and investigated the influence of Ce doping on the crystal phase, morphology, electronic structure, and photocatalytic activity of $ZnWO_4$. After the introduction of Ce atoms, the photocatalytic activity of $ZnWO_4$ improved with the increase in Ce content, owing to the following two reasons. First, the introduction of the Ce^{3+} dopant led to the generation of defects on the surface of Ce-doped $ZnWO_4$. Second, the Ce^{4+} ions on the surface of $ZnWO_4$ could efficiently trap electrons at the CB by the reduction of Ce^{4+} into Ce^{3+} ions, thus efficiently suppressing the recombination of photoinduced electrons and holes in the Ce-doped $ZnWO_4$. Therefore, rare earth elements with variable valence, such as Ce, La, and Eu, are promising dopants to improve the photocatalytic activity by trapping photogenerated electrons, consequently limiting the recombination of photogenerated charge carriers.

3.4 Heterojunction Fabrication

3.4.1 Hybridization with Semiconductors

Among the aforementioned approaches, constructing a semiconductor heterostructure is an effective means to obtain highly efficient photocatalysts [145–148]. When heterojunctions are composed of different semiconductors that have matching band potentials to form type-I or type-II heterojunctions through realignment of the energy level, the excited photogenerated holes and electrons can be moved from one semiconductor to another in opposite directions driven by the formed built-in electric fields [149, 150], thus strengthening the separation efficiency of the photoinduced electrons and holes and further enhancing photocatalytic performance.

For constructing MWO_4-based heterojunctions, semiconductors with a narrow band gap were chosen as a counterpart component to form the heterojunction system, which exhibited remarkable advantages for enhancing the photocatalytic performance. Among most semiconductors with a narrow band gap, cadmium sulfide (CdS) has attracted increasing attention for heterojunction fabrication because of its narrow band gap and high CB position, which could be beneficial for photocatalytic H_2 production [151, 152]. Therefore, various CdS/MWO_4 heterojunction photocatalysts have been developed, which exhibit enhanced photocatalytic activities in water purification and energy conversion [153, 154]. For instance, Yan et al. [155] prepared a CdS/$MnWO_4$ heterojunction using a facile hydrothermal method to mineralize MB and methyl violet (MV) under visible-light irradiation. Owing to the overlapping of energy bands and tightly contacted interfaces between CdS and $MnWO_4$, the holes at the VB of $MnWO_4$ could transfer to the VB of CdS, and the excited electrons at the CB of CdS could in turn move into the CB of $MnWO_4$. This model could efficiently limit the recombination rate of the photogenerated electrons and holes, thus intensifying the separation of the photogenerated charge carriers in the hybrid system (Fig. 14). Nevertheless, it is apparent that the introduced CdS amount was not synchronous with the photocatalytic activities of the heterojunction, while there was an optimal amount of CdS in the hybrid. Excessive CdS amounts caused severe agglomeration of $MnWO_4$, damaging the heterojunction and worsening the separation efficiency of the photogenerated electrons and holes. This phenomenon was nearly discovered in the heterojunctions by combining two or more components into one system. In addition, Xu et al. [156] prepared a CdS/$ZnWO_4$ heterojunction consisting of $ZnWO_4$ NRs and CdS NPs using a hydrothermal method for the photodegradation of ciprofloxacin antibiotics. Compared to the $ZnWO_4$ NRs and CdS NPs, the CdS/$ZnWO_4$ hybrids showed higher photocatalytic activity than bare $ZnWO_4$ NRs and CdS NPs, which was ascribed to the highly efficient separation of the photogenerated electrons and holes in the hybrid structure.

The CdS/$CdWO_4$ heterojunction also exhibited enhanced efficiency in the photocatalytic H_2 production. For instance, Jia [157] and Wang et al. [158] deposited CdS on the surface of $CdWO_4$ via an ion-exchange and in situ growth route, and the fabricated Z-scheme CdS/$CdWO_4$ hybrid exhibited significantly enhanced photocatalytic performance for H_2 evolution compared to that of the pure $CdWO_4$ and CdS. As discusses in the previous section, the MWO_4 with a small M^{2+} cation has a narrow band-gap energy, which can be considered an efficient solar energy harvester to connect with wide band-gap semiconductors for constructing MWO_4-based heterojunctions [159–161]. Thus, Jiang et al. [162] fabricated an $MnWO_4/TiO_2$ heterojunction with excellent mechanical adhesion by the in situ growth of $MnWO_4$ on a porous TiO_2 film; it presented extremely high photocatalytic performance for degrading MB because of its high crystallinity, large surface area, and strong mechanical properties (Fig. 15). Similarly, Buvaneswari et al. [163] prepared an $FeWO_4$/ZnO heterojunction via a simple co-precipitation route; the band gap of the prepared $FeWO_4$/ZnO heterojunction was estimated to be 2.12 eV, which was apparently smaller than that of ZnO (3.01 eV). In comparison to pristine ZnO, the photocatalytic activity of the $FeWO_4$/ZnO hybrid was substantially enhanced because of the formation of a $FeWO_4$/ZnO heterojunction structure. Additionally, the $CuWO_4$/ZnO hybrid consisting of ZnO NRs and $CuWO_4$ NPs fabricated by Mavric et al. [164] showed enhanced photocatalytic activity compared to that of pure $CuWO_4$ NPs and ZnO NRs.

Furthermore, a MO_x/MWO_4 hybrid as a smart-built heterojunction was fabricated using a facile one-pot synthetic strategy to enhance the interaction between MO_x and MWO_4, in which M is generally reported to be Fe, Ni, Co, or Cu [165–168]. Cao et al. [169] fabricated a novel p-n heterojunction consisting of Fe_3O_4 NPs and $FeWO_4$ nanowires. The calculated band gap of the $FeWO_4/Fe_3O_4$ heterojunction was 2.50 eV, lower than that of pristine $FeWO_4$ nanowires. The $FeWO_4/Fe_3O_4$ heterojunction exhibited enhanced photo-Fenton activity compared to that of the bare $FeWO_4$ nanowires under UV–visible-light irradiation with the addition of H_2O_2. In addition, a α-$SnWO_4/SnO_2$ heterostructure was synthesized with CTAB as the surfactant [170] and displayed enhanced photocatalytic performance compared to that of pure α-$SnWO_4$. Considering that WO_3 can be obtained by dehydration from tungstate acid, WO_3 is considered to be simultaneously produced during the synthesis of MWO_4 and is likely to form a MWO_4/WO_3 heterojunction, such as $CoWO_4/WO_3$

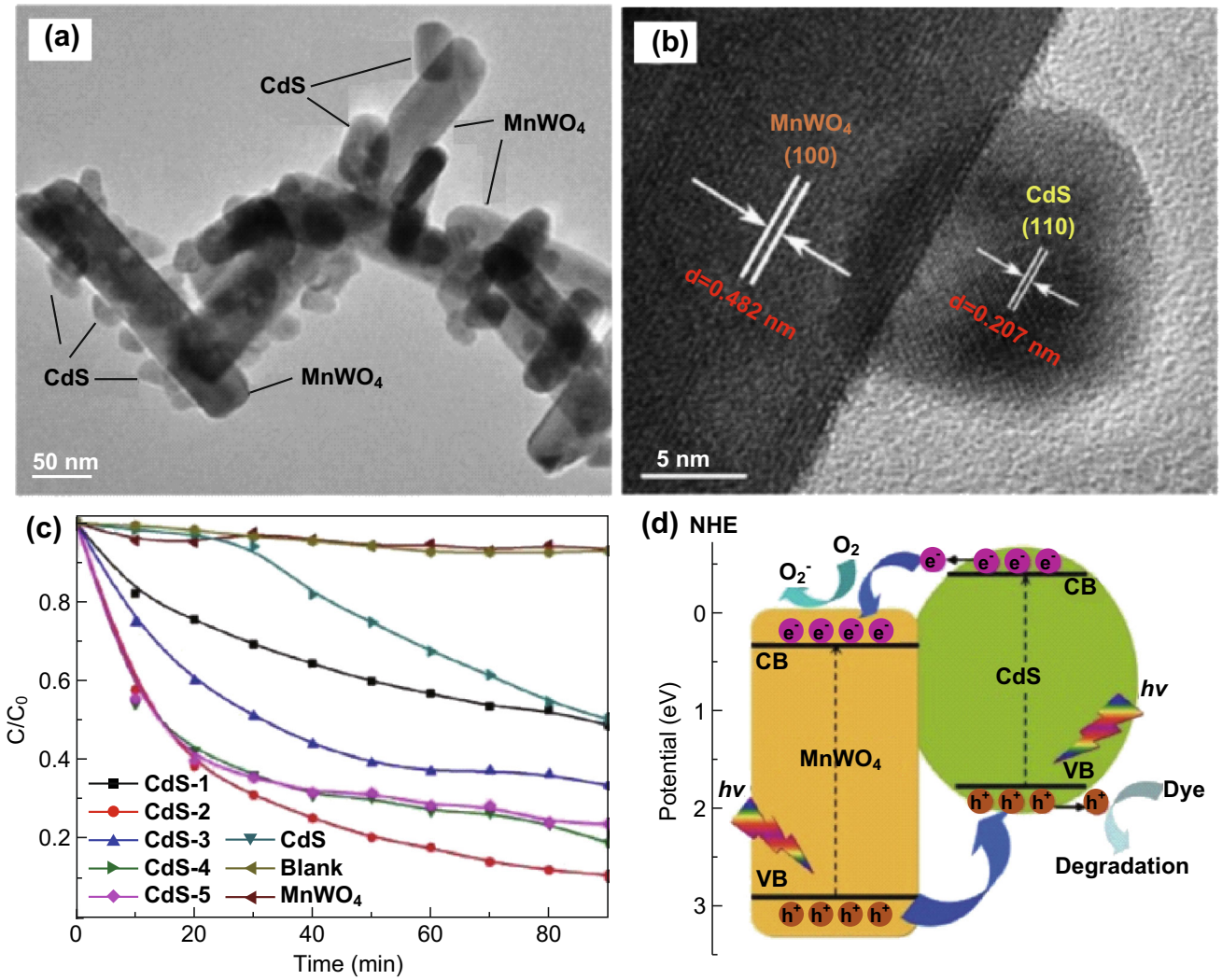

Fig. 14 **a**, **b** TEM and HRTEM images of a CdS/$MnWO_4$ heterojunction. **c** Photocatalytic degradation of MB over CdS/$MnWO_4$ with different CdS contents. **d** Schematic photocatalytic mechanism of CdS/$MnWO_4$ heterojunction. Reproduced with permission from Ref. [155]. Copyright 2017 Elsevier

[171, 172], $NiWO_4/WO_3$ [173, 174], or $CuWO_4/WO_3$ [175, 176]. Aslam et al. [177] prepared a $CdWO_4/WO_3$ heterojunction using a hydrothermal and chemisorption method, and reported enhanced photocatalytic activities toward the degradation of organic pollutants, compared with pure $CdWO_4$ and WO_3. This section clearly demonstrates in detail that the construction of MWO_4-based heterojunction systems is an effective and controllable method for enhancing the photocatalytic activities of MWO_4-based semiconductors.

3.4.2 Hybridization with Carbon-Rich Materials

Carbon-rich materials, including carbon nanotubes (CNTs), graphene, and graphitic carbon nitride (g-C_3N_4), possess unique physical and chemical properties such as a large surface area, high absorption co-efficiency, and chemical stability, ensuring excellent and long-lasting applications in the fields of photochemical and PEC water treatment, photovoltaic devices, and water splitting [178–183]. Carbon-rich materials have a conjugative π structure and unique sp^2/sp^3 hybrid carbon network, which are suitable substrates for constructing hybrid photocatalysts to intensify the separation and transportation of photoinduced charge carriers inside carbon-rich networks, thus improving the photocatalytic performance [184–187]. Based on this strategy, Gaillard et al. [188] synthesized a novel photoelectrode consisting of $CuWO_4$ and a multi-wall CNT (MWCNT) to tune the photogenerated charge transfer in the nanocomposite film for enhancing the performance of solar-driven PEC water splitting. Compared to the bare $CuWO_4$ photoelectrode, the resistance and photocurrent density of the $CuWO_4$/MWCNT composite photoelectrode decreased and increased by 30% and 26%, respectively.

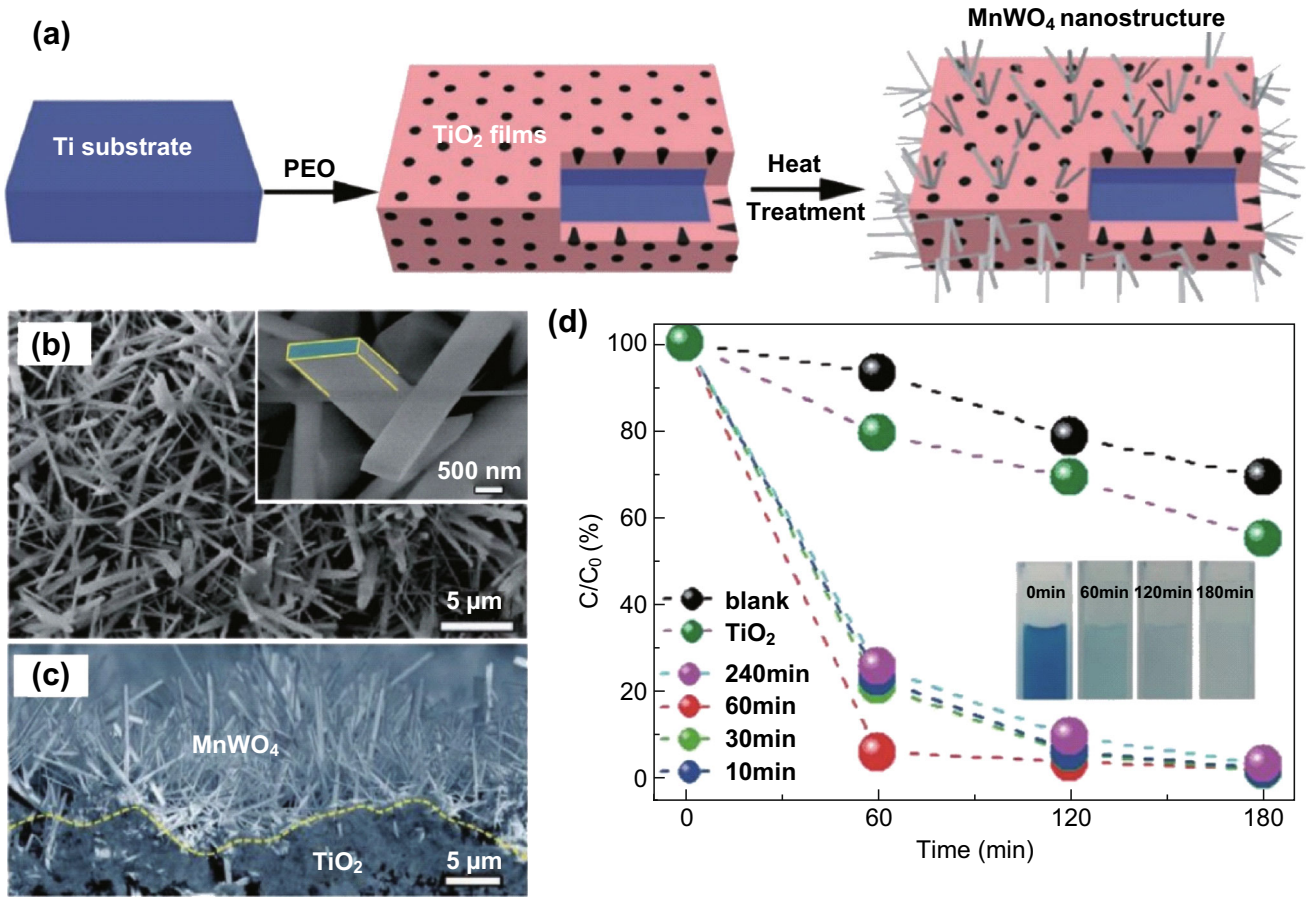

Fig. 15 **a** Schematic diagram describing the formation of $MnWO_4$ nanoplates. **b–c** FESEM images of the $MnWO_4$ nanoplates and $MnWO_4$ nanoplates on TiO_2 film. **d** Photodegradation efficiency of different samples heated at 850 °C for different times. Reproduced with permission from Ref. [162]. Copyright 2016 Royal Society of Chemistry

This was mainly attributed to the complete dispersion of the MWCNT as an electron collector in the entire $CuWO_4$ layer. Compared to CNTs, graphene nanosheets produced via the chemical oxidation treatment of graphite have more sp^3 hybridized edge structure because of the destroyed perfect sp^2 structure. It is well-known that a perfect sp^2 carbon structure (CNT) is beneficial for rapid charge mobility, and that an sp^3-hybridized carbon structure (graphene) can lead to a small band gap in the semiconductor [189, 190]. Meanwhile, layer-structure carbon materials have a richer porosity substructure assembly from graphene stacking and surface defects, which could provide more reactive sites, in comparison to tube-like carbon materials. Recently, Bai et al. [191] designed a $ZnWO_4$/graphene hybrid, demonstrating that graphene could act as a photo-sensitizer in the hybrid and improve the production of $^{\cdot}OH$ and $^{\cdot}O_2^-$ radicals. The excited photogenerated electrons at the CB of $ZnWO_4$ could be easily injected into the lowest unoccupied molecular orbital (LUMO) of graphene, resulting in a beneficial spatial separation between the holes and electrons inside the $ZnWO_4$/graphene hybrid, in which more holes and electrons can participate in the production of active species, in comparison to bare $ZnWO_4$. Xu et al. [192] reported a $CdWO_4$/graphene hybrid using a hydrothermal process, in which the formed heterojunction showed significantly enhanced photocatalytic activity compared to that of the bare $ZnWO_4$. However, it was found that excessive graphene could have a negative effect on the photocatalytic performance because of the reduced light absorption efficiency of $CdWO_4$ with the addition of the superfluous graphene.

Apart from graphene, other carbon-rich materials, such as g-C_3N_4 and mesoporous carbon materials, have been considered as promising candidates to build MWO_4-based heterojunctions. g-C_3N_4, which is regarded as an allotrope of C_3N_4, possesses excellent chemical stability, a suitable band gap of 2.7 eV, and a high specific surface area, which are beneficial for anchoring various other semiconductor materials [193–195]. For instance, Sun et al. [196] synthesized g-C_3N_4/$ZnWO_4$ NRs via a thermal treatment route, and investigated the microcosmic mechanisms of the

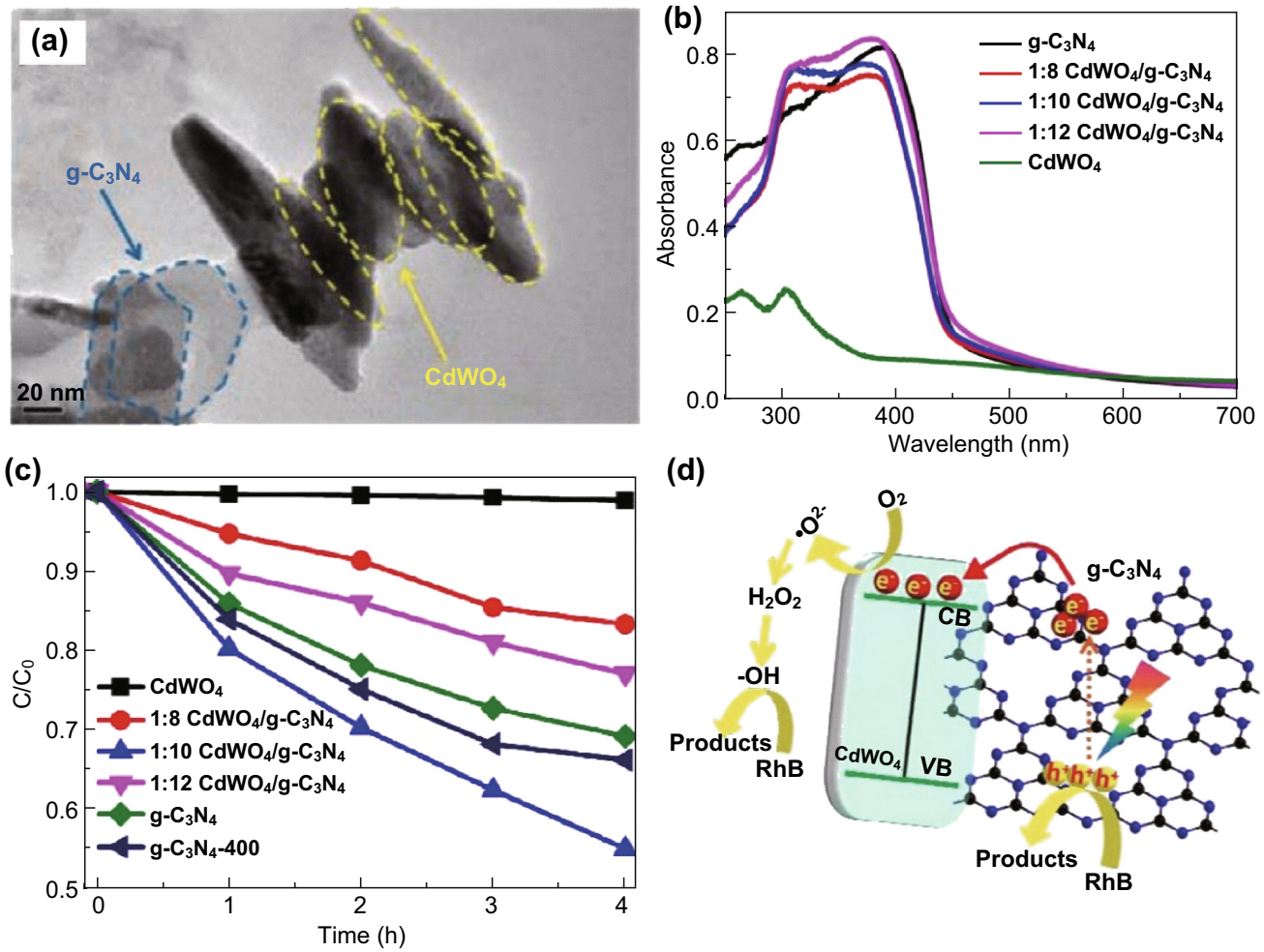

Fig. 16 **a** TEM image, **b** UV–vis diffused reflectance spectra, and **c** photocatalytic degradation curves of $CdWO_4/C_3N_4$. **d** Mechanism of photocatalytic reaction on the $CdWO_4/C_3N_4$. Reproduced with permission from Ref. [197]. Copyright 2015 Elsevier

enhanced photocatalytic activity of $C_3N_4/ZnWO_4$ in comparison to pristine $ZnWO_4$ NRs and C_3N_4. Together with theoretical calculation results, it was found that the well-matched energy level alignment of the C_3N_4 and $ZnWO_4$ NRs was the primary reason for the enhancement of the photocatalytic performance, in which the electrons at the VB top edge of the C_3N_4, when excited by the incident light, quickly jumped to the CB bottom edge of C_3N_4 and then transferred to the CB of $ZnWO_4$ because of the staged alignment, thus enhancing the charge transfer and separation efficiency. In addition, Tian et al. [197] synthesized a $CdWO_4/C_3N_4$ hybrid using a hydrothermal process, followed by a mixed-calcination treatment. Compared to pure $CdWO_4$, the $CdWO_4/C_3N_4$ heterojunction exhibited higher photocatalytic activity (Fig. 16c), the proposed mechanism for which is shown in Fig. 16d. The matched band structures between the two components contributed to the separation and transfer process, in which the excited electrons at the CB of C_3N_4 moved to the CB of $CdWO_4$ following a downward staged band, such that the photoinduced electrons and holes were efficiently separated, thus enhancing the overall photocatalytic activity. Considering its appropriate band energy level, g-C_3N_4 is usually used to construct a Z-scheme hybrid system to enhance photocatalytic activities. Instead of a type-II heterojunction, the direct Z-scheme configuration not only forms a built-in electronic field to promote the separation and transfer efficiency of photogenerated electrons and holes, but it also maintains the reductive and oxidative ability of electrons and holes [198, 199]. Recently, Zhu and co-workers [200] reported a direct Z-scheme heterojunction by combining g-C_3N_4 with Ag_2WO_4 through a facile precipitation route. Because of the use of g-C_3N_4 as a support in the precursor solution, Ag_2WO_4 was able to nucleate and grow on the surface of the layered C_3N_4, thus resulting in the Ag_2WO_4 evenly distributing on the surface of the layered g-C_3N_4-nanosheets. In comparison to the bare Ag_2WO_4 and g-C_3N_4, the Z-scheme of the g-C_3N_4/Ag_2WO_4 hybrid system exhibited

a much higher photoactivity for the degradation of MO, owing to the efficient separation between the photoinduced electrons and holes in the direct Z-scheme configuration. Given the aforementioned examples and explanations, it is obvious that carbon-rich materials possess a high charge carrier mobility and large specific surface area, which could efficiently promote the separation efficiency of photoexcited electrons and holes in the MWO_4, ultimately leading to improvement of the photocatalytic activity.

4 Summary and Outlook

This review summarized the development of novel strategies to enhance the photocatalytic performance of MWO_4-based materials with a special emphasis on their applications in environmental purification and solar water splitting. Although significant improvements have been achieved in the construction of highly efficient ternary MWO_4-based oxides, challenges remain that need to be addressed. First, the recombination rate of photogenerated charge carriers for MWO_4-based photocatalysts is still considerably high, accounting for poor reduction ability in the photoexcited electrons at a low potential of the CB edge, which are easily quenched by defects and holes. Second, although morphological engineering could improve the photocatalytic activity of MWO_4-based systems by regulating the crystal structure, particle size, and surface area, the current synthetic methods are inadequate for large-scale preparation, particularly for nanosized materials, which would significantly improve the separation efficiency of the photogenerated charge carriers. Third, the surface effect, particularly the crystal surface effect on the photocatalytic performance of MWO_4-based systems, has not been synergistically and comprehensively investigated. It is thought that the atom configurations and surface defects should be paid more attention, to provide important information for designing highly efficient photocatalysts. Fourth, based on this review, it is clear that the MWO_4 materials consisting of a single valence metal ion, such as Cd, Zn, or Sn, have been well-developed in the past, while those composed of a versatile valence metal, for instance, Co, Fe, or Ni, have been insufficiently explored in surface engineering and theoretical computation.

To overcome these challenges, future research needs to focus on the exploration of novel photocatalytic materials. Although the sunlight-harvesting ability and separation efficiency of photogenerated charge carriers could be strengthened by heteroatom doping or heterojunction fabrication as reported by previous literature, traditional material screening, high-throughput screening, and computational materials design can guide the construction of photocatalysts with a proper band edge position and suitable band gap, thereby shortening the experimental period, reducing the workload, and saving experimental cost. In other fundamental studies, combining experiment and theory would enable understanding the photocatalytic principles and screen alternative high-performance photocatalysts. Future work also needs to focus on facile synthetic approaches for constructing stable MWO_4 materials with high active crystal surface and/or quantum size, and developing advanced techniques for large-scale production. It is expected that further progress in ternary MWO_4-based photocatalysts for applications in environmental purification and solar water splitting will be made in future studies.

Acknowledgements Y. Hou thanks the support of NSFC 51702284, Fundamental Research Funds for the Central Universities (112109*172210171) and the Startup Foundation for Hundred-Talent Program of Zhejiang University (112100-193820101/001/022). J. Ke thanks the support of the NSFC 21501138, the Science Research Foundation of Wuhan Institute of Technology (K201513).

References

1. A. Fujishima, K. Honda, Electrochemical photolysis of water at a semiconductor electrode. Nature **238**, 37–38 (1972). https://doi.org/10.1038/238037a0
2. X.P. Chen, Z.X. Zhang, L. Chi, A.K. Nair, W.F. Shangguan, Z. Jiang, Recent advances in visible-light-driven photoelectrochemical water splitting: catalyst nanostructures and reaction systems. Nano-Micro Lett. **8**(1), 1–12 (2016). https://doi.org/10.1007/s40820-015-0063-3
3. Y. Hou, X. Li, Q. Zhao, G. Chen, C.L. Raston, Role of hydroxyl radicals and mechanism of Escherichia coli inactivation on Ag/AgBr/TiO_2 nanotube array electrode under visible light irradiation. Environ. Sci. Technol. **46**(7), 4042–4050 (2012). https://doi.org/10.1021/es204079d
4. L. Cheng, Q.J. Xiang, Y.L. Liao, H.W. Zhang, CdS-Based photocatalysts. Energ. Environ. Sci. **11**(6), 1362–1391 (2018). https://doi.org/10.1039/c7ee03640j
5. F. Wang, Q. Li, D. Xu, Recent progress in semiconductor-based nanocomposite photocatalysts for solar to chemical energy conversion. Adv. Energy Mater. **7**(23), 1700529 (2017). https://doi.org/10.1002/aenm.201700529
6. Y. Hou, X. Zhuang, X. Feng, Recent advances in earth-abundant heterogeneous electrocatalysts for photoelectrochemical water splitting. Small Methods **1**(6), 1700090 (2017). https://doi.org/10.1002/smtd.201700090
7. Y. Hou, X. Li, Q. Zhao, G. Chen, $ZnFe_2O_4$ multi-porous microbricks/graphene hybrid photocatalyst: facile synthesis, improved activity and photocatalytic mechanism. Appl. Catal. B Environ. **142–143**, 80–88 (2013). https://doi.org/10.1016/j.apcatb.2013.04.062
8. Y. Hou, X. Li, Q. Zhao, X. Quan, G. Chen, Electrochemically assisted photocatalytic degradation of 4-chlorophenol by

$ZnFe_2O_4$-modified TiO_2 nanotube array electrode under visible light irradiation. Environ. Sci. Technol. **44**(13), 5098–5103 (2010). https://doi.org/10.1021/es100004u
9. W.Y. Teoh, J.A. Scott, R. Amal, Progress in heterogeneous photocatalysis: from classical radical chemistry to engineering nanomaterials and solar reactors. J. Phys. Chem. Lett. **3**(5), 629–639 (2012). https://doi.org/10.1021/jz3000646
10. S. Banerjee, S.C. Pillai, P. Falaras, K.E. O'Shea, J.A. Byrne, D.D. Dionysiou, New insights into the mechanism of visible light photocatalysis. J. Phys. Chem. Lett. **5**(15), 2543–2554 (2014). https://doi.org/10.1021/jz501030x
11. J. Schneider, M. Matsuoka, M. Takeuchi, J. Zhang, Y. Horiuchi, M. Anpo, D.W. Bahnemann, Understanding TiO_2 photocatalysis: mechanisms and materials. Chem. Rev. **114**(19), 9919–9986 (2014). https://doi.org/10.1021/cr5001892
12. M.J. Kale, T. Avanesian, P. Christopher, Direct photocatalysis by plasmonic nanostructures. ACS Catal. **4**(1), 116–128 (2013). https://doi.org/10.1021/cs400993w
13. V. Augugliaro, G. Camera-Roda, V. Loddo, G. Palmisano, L. Palmisano, J. Soria, S. Yurdakal, Heterogeneous photocatalysis and photoelectrocatalysis: from unselective abatement of noxious species to selective production of high-value chemicals. J. Phys. Chem. Lett. **6**(10), 1968–1981 (2015). https://doi.org/10.1021/acs.jpclett.5b00294
14. S. Xie, Q. Zhang, G. Liu, Y. Wang, Photocatalytic and photoelectrocatalytic reduction of CO_2 using heterogeneous catalysts with controlled nanostructures. Chem. Commun. **52**(1), 35–59 (2016). https://doi.org/10.1039/c5cc07613g
15. A. García, C. Fernandez-Blanco, J.R. Herance, J. Albero, H. García, Graphenes as additives in photoelectrocatalysis. J. Mater. Chem. A **5**(32), 16522–16536 (2017). https://doi.org/10.1039/c7ta04045h
16. A.B. Laursen, S. Kegnæs, S. Dahl, I. Chorkendorff, Molybdenum sulfides-efficient and viable materials for electro- and photoelectrocatalytic hydrogen evolution. Energy Environ. Sci. **5**(2), 5577–5591 (2012). https://doi.org/10.1039/c2ee02618j
17. Y. Yang, S. Ajmal, X. Zheng, L. Zhang, Efficient nanomaterials for harvesting clean fuels from electrochemical and photoelectrochemical CO_2 reduction. Sustain. Energ. Fuels **2**(3), 510–537 (2018). https://doi.org/10.1039/c7se00371d
18. R. Zhou, R. Zhou, X. Zhang, J. Li, X. Wang et al., Synergistic effect of atmospheric-pressure plasma and TiO_2 photocatalysis on inactivation of Escherichia coli cells in aqueous media. Sci. Rep. **6**, 39552 (2016). https://doi.org/10.1038/srep39552
19. J.J. Zou, C.J. Liu, Y.P. Zhang, Control of the metal-support interface of NiO-loaded photocatalysts via cold plasma treatment. Langmuir **22**(5), 2334–2339 (2006). https://doi.org/10.1021/la052135u
20. L. Zhang, G. Kong, Y. Meng, J. Tian, L. Zhang, S. Wan, J. Lin, Y. Wang, Direct coupling of thermo- and photocatalysis for conversion of CO_2-H_2O into fuels. Chemsuschem **10**(23), 4709–4714 (2017). https://doi.org/10.1002/cssc.201701472
21. E.T. Kho, T.H. Tan, E. Lovell, R.J. Wong, J. Scott, R. Amal, A review on photo-thermal catalytic conversion of carbon dioxide. Green Energy Environ. **2**(3), 204–217 (2017). https://doi.org/10.1016/j.gee.2017.06.003
22. J. Jia, H. Wang, Z. Lu, P.G. O'Brien, M. Ghoussoub et al., Photothermal catalyst engineering: hydrogenation of gaseous CO_2 with high activity and tailored selectivity. Adv. Sci. **4**(10), 1700252 (2017). https://doi.org/10.1002/advs.201700252
23. H. Chen, C.E. Nanayakkara, V.H. Grassian, Titanium dioxide photocatalysis in atmospheric chemistry. Chem. Rev. **112**(11), 5919–5948 (2012). https://doi.org/10.1021/cr3002092
24. L. Wan, M. Long, D. Zhou, L. Zhang, W. Cai, Preparation and characterization of freestanding hierarchical porous TiO_2 monolith modified with graphene oxide. Nano-Micro Lett. **4**(2), 90–97 (2012). https://doi.org/10.1007/bf03353698
25. M. Boehme, W. Ensinger, Mixed phase anatase/rutile titanium dioxide nanotubes for enhanced photocatalytic degradation of methylene blue. Nano-Micro Lett. **3**(4), 236–241 (2011). https://doi.org/10.1007/bf03353678
26. X. Li, J. Li, J. Bai, Y. Dong, L. Li, B. Zhou, The inhibition effect of tert-butyl alcohol on the TiO_2 nano assays photoelectrocatalytic degradation of different organics and its mechanism. Nano-Micro Lett. **8**(3), 221–231 (2016). https://doi.org/10.1007/s40820-015-0080-2
27. X. Li, Y. Jiang, W. Cheng, Y. Li, X. Xu, K. Lin, Mesoporous TiO_2/carbon beads: one-pot preparation and their application in visible-light-induced photodegradation. Nano-Micro Lett. **7**(3), 243–254 (2015). https://doi.org/10.1007/s40820-015-0029-5
28. Y. Hou, F. Zuo, A. Dagg, P. Feng, Visible light-driven α-Fe_2O_3 nanorod/graphene/$BiV_{1-x}Mo_xO_4$ core/shell heterojunction array for efficient photoelectrochemical water splitting. Nano Lett. **12**(12), 6464–6473 (2012). https://doi.org/10.1021/nl303961c
29. J. Ke, H. Zhou, J. Liu, X. Duan, H. Zhang, S. Liu, S. Wang, Crystal transformation of 2D tungstic acid H_2WO_4 to WO_3 for enhanced photocatalytic water oxidation. J. Colloid Interface Sci. **514**, 576–583 (2018). https://doi.org/10.1016/j.jcis.2017.12.066
30. Y. Hou, F. Zuo, A.P. Dagg, J. Liu, P. Feng, Branched WO_3 nanosheet array with layered C_3N_4 heterojunctions and CoO_x nanoparticles as a flexible photoanode for efficient photoelectrochemical water oxidation. Adv. Mater. **26**(29), 5043–5049 (2014). https://doi.org/10.1002/adma.201401032
31. S. Luo, J. Ke, M. Yuan, Q. Zhang, P. Xie, L. Deng, S. Wang, $CuInS_2$ quantum dots embedded in Bi_2WO_6 nanoflowers for enhanced visible light photocatalytic removal of contaminants. Appl. Catal. B: Environ. **221**, 215–222 (2018). https://doi.org/10.1016/j.apcatb.2017.09.028
32. S.G. Kumar, K.S.R.K. Rao, Zinc oxide based photocatalysis: tailoring surface-bulk structure and related interfacial charge carrier dynamics for better environmental applications. RSC Adv. **5**(5), 3306–3351 (2015). https://doi.org/10.1039/c4ra13299h
33. J. Ke, J. Liu, H. Sun, H. Zhang, X. Duan et al., Facile assembly of Bi_2O_3/Bi_2S_3/MoS_2 n-p heterojunction with layered n-Bi_2O_3 and p-MoS_2 for enhanced photocatalytic water oxidation and pollutant degradation. Appl. Catal. B: Environ. **200**, 47–55 (2017). https://doi.org/10.1016/j.apcatb.2016.06.071
34. J. Liu, Y. Li, J. Ke, S. Wang, L. Wang, H. Xiao, Black NiO-TiO_2 nanorods for solar photocatalysis: recognition of electronic structure and reaction mechanism. Appl. Catal. B: Environ. **224**, 705–714 (2018). https://doi.org/10.1016/j.apcatb.2017.11.028
35. S.G. Kumar, L.G. Devi, Review on modified TiO_2 photocatalysis under UV/visible light: selected results and related mechanisms on interfacial charge carrier transfer dynamics. J. Phys. Chem. A **115**(46), 13211–13241 (2011). https://doi.org/10.1021/jp204364a
36. M. Ni, M.K.H. Leung, D.Y.C. Leung, K. Sumathy, A review and recent developments in photocatalytic water-splitting using TiO_2 for hydrogen production. Renew. Sustain. Energ. Rev. **11**(3), 401–425 (2007). https://doi.org/10.1016/j.rser.2005.01.009
37. J. Ke, X. Li, Q. Zhao, B. Liu, S. Liu, S. Wang, Upconversion carbon quantum dots as visible light responsive component for efficient enhancement of photocatalytic performance. J. Colloid Interface Sci. **496**, 425–433 (2017). https://doi.org/10.1016/j.jcis.2017.01.121
38. A. Fujishima, X. Zhang, D. Tryk, Heterogeneous photocatalysis: from water photolysis to applications in environmental cleanup.

Int. J. Hydrog. Energy **32**(14), 2664–2672 (2007). https://doi.org/10.1016/j.ijhydene.2006.09.009
39. X. Zou, Y. Dong, S. Li, J. Ke, Y. Cui, Facile anion exchange to construct uniform AgX (X = Cl, Br, I)/Ag2CrO4 NR hybrids for efficient visible light driven photocatalytic activity. Sol. Energy **169**, 392–400 (2018). https://doi.org/10.1016/j.solener.2018.05.017
40. M.R. Hoffmann, S.T. Martin, W.Y. Choi, D.W. Bahnemann, Environmental applications of semiconductor photocatalysis. Chem. Rev. **95**(28), 69–96 (1995). https://doi.org/10.1021/cr00033a004
41. D. Chen, X.G. Zhang, A.F. Lee, Synthetic strategies to nanostructured photocatalysts for CO_2 reduction to solar fuels and chemicals. J. Mater. Chem. A **3**(28), 14487–14516 (2015). https://doi.org/10.1039/c5ta01592h
42. H.F. Cheng, K. Fuku, Y. Kuwahara, K. Mori, H. Yamashita, Harnessing single-active plasmonic nanostructures for enhanced photocatalysis under visible light. J. Mater. Chem. A **3**(10), 5244–5258 (2015). https://doi.org/10.1039/c4ta06484d
43. K. Wenderich, G. Mul, Methods, mechanism, and applications of photodeposition in photocatalysis: a review. Chem. Rev. **116**(23), 14587–14619 (2016). https://doi.org/10.1021/acs.chemrev.6b00327
44. T. Hisatomi, J. Kubota, K. Domen, Recent advances in semiconductors for photocatalytic and photoelectrochemical water splitting. Chem. Soc. Rev. **43**(22), 7520–7535 (2014). https://doi.org/10.1039/c3cs60378d
45. G. Zhang, G. Liu, L. Wang, J.T.S. Irvine, Inorganic perovskite photocatalysts for solar energy utilization. Chem. Soc. Rev. **45**(21), 5951–5984 (2016). https://doi.org/10.1039/c5cs00769k
46. D.M. Fabian, S. Hu, N. Singh, F.A. Houle, T. Hisatomi, K. Domen, F.E. Osterloh, S. Ardo, Particle suspension reactors and materials for solar-driven water splitting. Energy Environ. Sci. **8**(10), 2825–2850 (2015). https://doi.org/10.1039/c5ee01434d
47. T. Takata, K. Domen, Development of non-oxide semiconductors as light harvesting materials in photocatalytic and photoelectrochemical water splitting. Dalton Trans. **46**(32), 10529–10544 (2017). https://doi.org/10.1039/c7dt00867h
48. P. Mal, G. Bera, P. Rambabu, G.R. Turpu, B. Chakraborty et al., Electronic, magnetic and spectroscopic properties of doped $Mn_{(1-x)}$ A_xWO_4 (A = Co, Cu, Ni and Fe) multiferroic: an experimental and DFT study. J. Phys. Condens. Matter **29**(7), 075901 (2017). https://doi.org/10.1088/1361-648X/aa4e64
49. S.M.M. Zawawi, R. Yahya, Z. Hassan, E.H.N.M. Ekramul Mahmud, N.M. Daud, Structural and optical characterization of metal tungstates (MWO_4; M = Ni, Ba, Bi) synthesized by a sucrose-templated method. Chem. Cent. J. **7**, 80 (2013). https://doi.org/10.1186/1752-153X-7-80
50. X.A. López, A.F. Fuentes, M.M. Zaragoza, J.A. Díaz Guillén, J.S. Gutiérrez, A.L. Ortiz, V. Collins-Martínez, Synthesis, characterization and photocatalytic evaluation of MWO4 (M = Ni Co, Cu and Mn) tungstates. Int. J. Hydrog. Energy **41**(48), 23312–23317 (2016). https://doi.org/10.1016/j.ijhydene.2016.10.117
51. S. Dey, R.A. Ricciardo, H.L. Cuthbert, P.M. Woodward, Metal-to-metal charge transfer in AWO4 (A = Mg, Mn Co, Ni, Cu, or Zn) compounds with the wolframite structure. Inorg. Chem. **53**(9), 4299–4394 (2014). https://doi.org/10.1021/ic4031798
52. M. Nikl, P. Bohacek, E. Mihokova, M. Kobayashi, M. Ishii et al., Excitonic emission of scheelite tungstates AWO_4 (A = Pb, Ca, Ba, Sr). J. Lumin. **87–89**, 1136–1139 (2000). https://doi.org/10.1016/S0022-2313(99)00569-4
53. R.C. Pullar, S. Farrah, N.M. Alford, $MgWO_4$, $ZnWO_4$, $NiWO_4$ and $CoWO_4$ microwave dielectric ceramics. J. Eur. Ceram. Soc. **27**(2–3), 1059–1063 (2007). https://doi.org/10.1016/j.jeurceramsoc.2006.05.085
54. G. Zhang, R. Jia, Q. Wu, Preparation, structural and optical properties of AWO_4 (A = Ca, Ba, Sr) nanofilms. Mater. Sci. Eng. B **128**(1–3), 254–259 (2006). https://doi.org/10.1016/j.mseb.2005.11.040
55. R. Lacomba-Perales, J. Ruiz-Fuertes, D. Errandonea, D. Martínez-García, A. Segura, Optical absorption of divalent metal tungstates: correlation between the band-gap energy and the cation ionic radius. EPL **83**(3), 37002 (2008). https://doi.org/10.1209/0295-5075/83/37002
56. C. Shivakumara, R. Saraf, S. Behera, N. Dhananjaya, H. Nagabhushana, Scheelite-type MWO_4 (M = Ca, Sr, and Ba) nanophosphors: facile synthesis, structural characterization, photoluminescence, and photocatalytic properties. Mater. Res. Bull. **61**, 422–432 (2015). https://doi.org/10.1016/j.materresbull.2014.09.096
57. S.D. Ramarao, S. Roopas Kiran, V.R.K. Murthy, Structural, lattice vibrational, optical and microwave dielectric studies on $Ca_{1-x}Sr_xMoO_4$ ceramics with scheelite structure. Mater. Res. Bull. **56**, 71–79 (2014). https://doi.org/10.1016/j.materresbull.2014.04.064
58. Y.G. Su, G.S. Li, Y.F. Xue, L.P. Li, Tunable physical properties of $CaWO_4$ nanocrystals via particle size control. J. Phys. Chem. C **111**(18), 6684–6689 (2007). https://doi.org/10.1021/jp068480p
59. S.M. Ghoreishi, Facile synthesis and characterization of $CaWO_4$ nanoparticles using a new Schiff base as capping agent: enhanced photocatalytic degradation of methyl orange. J. Mater. Sci. Mater. Electron. **28**(19), 14833–14838 (2017). https://doi.org/10.1007/s10854-017-7354-z
60. M. Mohamed Jaffer Sadiq, A. Samson Nesaraj, Soft chemical synthesis and characterization of $BaWO_4$ nanoparticles for photocatalytic removal of Rhodamine B present in water sample. J. Nanostruct. Chem. **5**(1), 45–54 (2014). https://doi.org/10.1007/s40097-014-0133-y
61. M.C. Oliveira, L. Gracia, I.C. Nogueira, M.F.D. Carmo Gurgel, J.M.R. Mercury, E. Longo, J. Andrés, Synthesis and morphological transformation of $BaWO_4$ crystals: experimental and theoretical insights. Ceram. Int. **42**(9), 10913–10921 (2016). https://doi.org/10.1016/j.ceramint.2016.03.225
62. C. Yu, F. Cao, X. Li, G. Li, Y. Xie, J.C. Yu, Q. Shu, Q. Fan, J. Chen, Hydrothermal synthesis and characterization of novel $PbWO_4$ microspheres with hierarchical nanostructures and enhanced photocatalytic performance in dye degradation. Chem. Eng. J. **219**, 86–95 (2013). https://doi.org/10.1016/j.cej.2012.12.064
63. D. Chen, Z. Liu, S.X. Ouyang, J.H. Ye, Simple room-temperature mineralization method to $SrWO_4$ micro/nanostructures and their photocatalytic properties. J. Phys. Chem. C **115**(32), 15778–15784 (2011). https://doi.org/10.1021/jp202406n
64. D. Ye, D.Z. Li, W.J. Zhang, M. Sun, Y. Hu, Y.F. Zhang, X.Z. Fu, A new photocatalyst $CdWO_4$ prepared with a hydrothermal method. J. Phys. Chem. C **112**(44), 17351–17356 (2008). https://doi.org/10.1021/jp8059213
65. A.M. Priya, R.K. Selvan, B. Senthilkumar, M.K. Satheeshkumar, C. Sanjeeviraja, Synthesis and characterization of $CdWO_4$ nanocrystals. Ceram. Int. **37**(7), 2485–2488 (2011). https://doi.org/10.1016/j.ceramint.2011.03.040
66. C. Zhang, H. Zhang, K. Zhang, X. Li, Q. Leng, C. Hu, Photocatalytic activity of $ZnWO_4$: band structure, morphology and surface modification. ACS Appl. Mater. Interfaces **6**(16), 14423–14432 (2014). https://doi.org/10.1021/am503696b
67. J. Guo, X. Zhou, Y. Lu, X. Zhang, S. Kuang, W. Hou, Monodisperse spindle-like $FeWO_4$ nanoparticles: controlled hydrothermal synthesis and enhanced optical properties. J. Solid State Chem. **196**, 550–556 (2012). https://doi.org/10.1016/j.jssc.2012.07.026

68. M. Sivakumar, R. Madhu, S.M. Chen, V. Veeramani, A. Manikandan, W.H. Hung, N. Miyamoto, Y.L. Chueh, Low-temperature chemical synthesis of $CoWO_4$ nanospheres for sensitive nonenzymatic glucose sensor. J. Phys. Chem. C **120**(30), 17024–17028 (2016). https://doi.org/10.1021/acs.jpcc.6b04116
69. F. Ahmadi, M. Rahimi-Nasrabadi, M. Eghbali-Arani, The synthesize of $CuWO_4$ nanoparticles by a new morphological control method, characterization of its photocatalytic activity. J. Mater. Sci. Mater. Electron. **28**(7), 5244–5249 (2016). https://doi.org/10.1007/s10854-016-6181-y
70. M. Vosoughifar, Preparation, characterization, and morphological control of $MnWO_4$ nanoparticles through novel method and its photocatalyst application. J. Mater. Sci. Mater. Electron. **28**(2), 2135–2140 (2016). https://doi.org/10.1007/s10854-016-5777-6
71. R. Karthiga, B. Kavitha, M. Rajarajan, A. Suganthi, Photocatalytic and antimicrobial activity of $NiWO_4$ nanoparticles stabilized by the plant extract. Mater. Sci. Semicond. Process. **40**, 123–129 (2015). https://doi.org/10.1016/j.mssp.2015.05.037
72. G. Zhu, W. Que, J. Zhang, P. Zhong, Photocatalytic activity of $SnWO_4$ and SnW_3O_9 nanostructures prepared by a surfactant-assisted hydrothermal process. Mater. Sci. Eng. B **176**(18), 1448–1455 (2011). https://doi.org/10.1016/j.mseb.2011.08.003
73. S. Pourmasoud, M. Eghbali-Arani, F. Ahmadi, M. Rahimi-Nasrabadi, Synthesis, characterization, and morphological control of $PbWO_4$ nanostructures through precipitation method and its photocatalyst application. J. Mater. Sci. Mater. Electron. **28**(22), 17089–17097 (2017). https://doi.org/10.1007/s10854-017-7635-6
74. W.M. Tong, L.P. Li, W.B. Hu, T.J. Yan, G.S. Li, Systematic control of monoclinic $CdWO_4$ nanophase for optimum photocatalytic activity. J. Phys. Chem. C **114**(3), 1512–1519 (2010). https://doi.org/10.1021/jp910284u
75. S.M. Hosseinpour-Mashkani, M. Maddahfar, A. Sobhani-Nasab, Precipitation synthesis, characterization, morphological control, and photocatalyst application of $ZnWO_4$ nanoparticles. J. Electron. Mater. **45**(7), 3612–3620 (2016). https://doi.org/10.1007/s11664-016-4532-3
76. S.M. Hosseinpour-mashkani, A. Sobhani-Nasab, Simple synthesis and characterization of copper tungstate nanoparticles: investigation of surfactant effect and its photocatalyst application. J. Mater. Sci. Mater. Electron. **27**(7), 7548–7553 (2016). https://doi.org/10.1007/s10854-016-4735-7
77. S. Wannapop, T. Thongtem, S. Thongtem, Photoemission and energy gap of $MgWO_4$ particles connecting as nanofibers synthesized by electrospinning-calcination combinations. Appl. Surf. Sci. **258**(11), 4971–4976 (2012). https://doi.org/10.1016/j.apsusc.2012.01.133
78. A.T. Raj, S. Thangavel, A. Rose, C.V. Jipsa, M. Jose, G. Nallamuthu, S.J. Kim, G. Venugopal, Influence of morphology and common oxidants on the photocatalytic property of β-$SnWO_4$ nanoparticles. J. Nanosci. Nanotechnol. **16**(3), 2541–2547 (2016). https://doi.org/10.1166/jnn.2016.10961
79. W.M. Tong, L.P. Li, W.B. Hu, T.J. Yan, X.F. Guan, G.S. Li, Kinetic control of $MnWO_4$ nanoparticles for tailored structural properties. J. Phys. Chem. C **114**(36), 15298–15305 (2010). https://doi.org/10.1021/jp103879c
80. M.I. Ahmed, A. Adam, A. Khan, A.U. Rehman, M. Qamaruddin, M.N. Siddiqui, M. Qamar, Improved photoelectrochemical water oxidation under visible light with mesoporous $CoWO_4$. Mater. Lett. **183**, 281–284 (2016). https://doi.org/10.1016/j.matlet.2016.07.137
81. Q. Gao, Z. Liu, $FeWO_4$ nanorods with excellent UV-Visible light photocatalysis. Prog. Nat. Sci. Mater. **27**(5), 556–560 (2017). https://doi.org/10.1016/j.pnsc.2017.08.016
82. J. Di, J. Xiong, H. Li, Z. Liu, Ultrathin 2D photocatalysts: electronic-structure tailoring, hybridization, and applications. Adv. Mater. **30**(1), 1704548 (2018). https://doi.org/10.1002/adma.201704548
83. T. Yan, L. Li, W. Tong, J. Zheng, Y. Wang, G. Li, $CdWO_4$ polymorphs: selective preparation, electronic structures, and photocatalytic activities. J. Solid State Chem. **184**(2), 357–364 (2011). https://doi.org/10.1016/j.jssc.2010.12.013
84. L.G. Cai, F.M. Liu, D. Zhang, W.W. Zhong, Dependence of optical properties of monoclinic $MnWO_4$ on the electric field of incident light. Phys. B **407**(17), 3654–3659 (2012). https://doi.org/10.1016/j.physb.2012.05.044
85. S.M. Hosseinpour-Mashkani, A. Sobhani-Nasab, A simple sonochemical synthesis and characterization of $CdWO_4$ nanoparticles and its photocatalytic application. J. Mater. Sci. Mater. Electron. **27**(4), 3240–3244 (2015). https://doi.org/10.1007/s10854-015-4150-5
86. Y. Wang, X. Guan, L. Li, H. Lin, X. Wang, G. Li, Solvent-driven polymorphic control of $CdWO_4$ nanocrystals for photocatalytic performances. New J. Chem. **36**(9), 1852–1858 (2012). https://doi.org/10.1039/c2nj40504k
87. M. Dan, M. Cheng, H. Gao, H. Zheng, C. Feng, Synthesis and electrochemical properties of $SnWO_4$. J. Nanosci. Nanotechnol. **14**(3), 2395–2399 (2014). https://doi.org/10.1166/jnn.2014.8497
88. I.S. Cho, C.H. Kwak, D.W. Kim, S.W. Lee, K.S. Hong, Photophysical, photoelectrochemical, and photocatalytic properties of novel $SnWO_4$ oxide semiconductors with narrow band gaps. J. Phys. Chem. C **113**(24), 10647–10653 (2009). https://doi.org/10.1021/jp901557z
89. D. Chen, L. Gao, A. Yasumori, K. Kuroda, Y. Sugahara, Size- and shape-controlled conversion of tungstate-based inorganic-organic hybrid belts to WO_3 nanoplates with high specific surface areas. Small **4**(10), 1813–1822 (2008). https://doi.org/10.1002/smll.200800205
90. L. Liang, J. Zhang, Y. Zhou, J. Xie, X. Zhang, M. Guan, B. Pan, Y. Xie, High-performance flexible electrochromic device based on facile semiconductor-to-metal transition realized by $WO_3 \cdot 2H_2O$ ultrathin nanosheets. Sci. Rep. **3**, 1936 (2013). https://doi.org/10.1038/srep01936
91. Z.F. Huang, J. Song, L. Pan, X. Zhang, L. Wang, J.J. Zou, Tungsten oxides for photocatalysis, electrochemistry, and phototherapy. Adv. Mater. **27**(36), 5309–5327 (2015). https://doi.org/10.1002/adma.201501217
92. Y. Abraham, N.A.W. Holzwarth, R.T. Williams, Electronic structure and optical properties of $CdMoO_4$ and $CdWO_4$. Phys. Rev. B **62**(3), 1733–1741 (2000). https://doi.org/10.1103/PhysRevB.62.1733
93. S. Shepard, M. Smeu, Ab initio study of structural and electronic properties of copper and nickel tungstate. Comput. Mater. Sci. **143**, 301–307 (2018). https://doi.org/10.1016/j.commatsci.2017.11.021
94. A.E.B. Lima, M.J.S. Costa, R.S. Santos, N.C. Batista, L.S. Cavalcante, E. Longo, G.E. Luz, Facile preparation of $CuWO_4$ porous films and their photoelectrochemical properties. Electrochim. Acta **256**, 139–145 (2017). https://doi.org/10.1016/j.electacta.2017.10.010
95. L. Wang, F. Ke, Q. Wang, J. Yan, C. Liu et al., Effect of crystallization water on the structural and electrical properties of $CuWO_4$ under high pressure. Appl. Phys. Lett. **107**(20), 201603 (2015). https://doi.org/10.1063/1.4935978
96. D. Wang, P.S. Bassi, H. Qi, X. Zhao, Gurudayal, L.H. Wong, R. Xu, T. Sritharan, Z. Chen, Improved charge separation in WO_3/$CuWO_4$ composite photoanodes for photoelectrochemical water oxidation. Materials **9**(5), 348 (2016). https://doi.org/10.3390/ma9050348

97. S. Sun, W. Wang, Advanced chemical compositions and nanoarchitectures of bismuth based complex oxides for solar photocatalytic application. RSC Adv. **4**(88), 47136–47152 (2014). https://doi.org/10.1039/c4ra06419d
98. V.V. Atuchin, B.I. Troitskaia, O.Y. Khyzhun, V.L. Bekenev, Y.M. Solonin, Electronic properties of h-WO_3 and $CuWO_4$ nanocrystals as determined from X-ray spectroscopy and first principles band structure calculations. Int. J. Appl. Phys. Math. **1**(1), 19–23 (2011). https://doi.org/10.7763/ijapm.2011.V1.4
99. O.Y. Khyzhun, V.L. Bekenev, Y.M. Solonin, First-principles calculations and X-ray spectroscopy studies of the electronic structure of $CuWO_4$. J. Alloy. Compd. **480**(2), 184–189 (2009). https://doi.org/10.1016/j.jallcom.2009.01.119
100. O.Y. Khyzhun, T. Strunskus, S. Cramm, Y.M. Solonin, Electronic structure of $CuWO_4$: XPS, XES and NEXAFS studies. J. Alloy. Compd. **389**(1–2), 14–20 (2005). https://doi.org/10.1016/j.jallcom.2004.08.013
101. M.V. Lalić, Z.S. Popović, F.R. Vukajlović, Ab initio study of electronic, magnetic and optical properties of $CuWO_4$ tungstate. Comp. Mater. Sci. **50**(3), 1179–1186 (2011). https://doi.org/10.1016/j.commatsci.2010.11.018
102. C.R. Lhermitte, B.M. Bartlett, Advancing the chemistry of $CuWO_4$ for photoelectrochemical water oxidation. Acc. Chem. Res. **49**(6), 1121–1129 (2016). https://doi.org/10.1021/acs.accounts.6b00045
103. S. Rajagopal, D. Nataraj, O.Y. Khyzhun, Y. Djaoued, J. Robichaud, D. Mangalaraj, Hydrothermal synthesis and electronic properties of $FeWO_4$ and $CoWO_4$ nanostructures. J. Alloy. Compd. **493**(1–2), 340–345 (2010). https://doi.org/10.1016/j.jallcom.2009.12.099
104. S. Rajagopal, V.L. Bekenev, D. Nataraj, D. Mangalaraj, O.Y. Khyzhun, Electronic structure of $FeWO_4$ and $CoWO_4$ tungstates: first-principles FP-LAPW calculations and X-ray spectroscopy studies. J. Alloy. Compd. **496**(1–2), 61–68 (2010). https://doi.org/10.1016/j.jallcom.2010.02.107
105. K. Hoang, M. Oh, Y. Choi, Electronic structure, polaron formation, and functional properties in transition-metal tungstates. RSC Adv. **8**(8), 4191–4196 (2018). https://doi.org/10.1039/c7ra13436c
106. F. Yu, L. Cao, J. Huang, J. Wu, Effects of pH on the microstructures and optical property of $FeWO_4$ nanocrystallites prepared via hydrothermal method. Ceram. Int. **39**(4), 4133–4138 (2013). https://doi.org/10.1016/j.ceramint.2012.10.269
107. L. Hou, L. Lian, L. Zhang, T. Wu, C. Yuan, Microwave-assisted interfacial hydrothermal fabrication of hydrophobic $CdWO_4$ microspheres as a high-performance photocatalyst. RSC Adv. **4**(5), 2374–2381 (2014). https://doi.org/10.1039/c3ra45784b
108. Y. Ling, L. Zhou, L. Tan, Y. Wang, C. Yu, Synthesis of urchin-like $CdWO_4$ microspheres via a facile template free hydrothermal method. CrystEngComm **12**(10), 3019–3026 (2010). https://doi.org/10.1039/b927420k
109. S. Kang, Y. Li, M. Wu, M. Cai, P.K. Shen, Synthesis of hierarchically flower-like $FeWO_4$ as high performance anode materials for Li-ion batteries by a simple hydrothermal process. Int. J. Hydrog. Energy **39**(28), 16081–16087 (2014). https://doi.org/10.1016/j.ijhydene.2014.02.101
110. S. Liu, S. Tian, R. Xing, $CaWO_4$ hierarchical nanostructures: hydrothermal synthesis, growth mechanism and photoluminescence properties. CrystEngComm **13**(24), 7258–7261 (2011). https://doi.org/10.1039/c1ce05790a
111. T.N. Kovács, G. Pokol, F. Gáber, D. Nagy, T. Igricz, I.E. Lukács, Z. Fogarassy, K. Balázsi, I.M. Szilágyi, Preparation of iron tungstate ($FeWO_4$) nanosheets by hydrothermal method. Mater. Res. Bull. **95**, 563–569 (2017). https://doi.org/10.1016/j.materresbull.2017.08.031
112. Z.G. Chen, H.J. Ma, J.X. Xia, J. Zeng, J. Di, S. Yin, L. Xu, H.M. Li, Ionic liquid-induced strategy for $FeWO_4$ microspheres with advanced visible light photocatalysis. Ceram. Int. **42**(7), 8997–9003 (2016). https://doi.org/10.1016/j.ceramint.2016.02.117
113. Y.X. Zhou, Q. Zhang, J.Y. Gong, S.H. Yu, Surfactant-assisted hydrothermal synthesis and magnetic properties of urchin-like $MnWO_4$ microspheres. J. Phys. Chem. C **112**(35), 13383–13389 (2008). https://doi.org/10.1021/jp804211w
114. Y. Xing, S. Song, J. Feng, Y. Lei, M. Li, H. Zhang, Microemulsion-mediated solvothermal synthesis and photoluminescent property of 3D flowerlike $MnWO_4$ micro/nanocomposite structure. Solid State Sci. **10**(10), 1299–1304 (2008). https://doi.org/10.1016/j.solidstatesciences.2008.01.019
115. Y.C. Chen, Y.G. Lin, L.C. Hsu, A. Tarasov, P.T. Chen, M. Hayashi, J. Ungelenk, Y.K. Hsu, C. Feldmann, β-$SnWO_4$ photocatalyst with controlled morphological transition of cubes to spikecubes. ACS Catal. **6**(4), 2357–2367 (2016). https://doi.org/10.1021/acscatal.5b02444
116. X.Y. Qiu, H.W. Huang, Y.D. Gao, Effects of surface properties of 010}, {001 and 100 of MnWO4 and FeWO4 on absorption of collector. Appl. Surf. Sci. **367**, 354–361 (2016). https://doi.org/10.1016/j.apsusc.2016.01.190
117. J. Ungelenk, C. Feldmann, Synthesis of faceted beta-$SnWO_4$ microcrystals with enhanced visible-light photocatalytic properties. Chem. Commun. **48**(63), 7838–7840 (2012). https://doi.org/10.1039/c2cc33224h
118. T. Tian, L. Ai, X. Liu, L. Li, J. Li, J. Jiang, Synthesis of hierarchical $FeWO_4$ architectures with {100}-faceted nanosheet assemblies as a robust biomimetic catalyst. Ind. Eng. Chem. Res. **54**(4), 1171–1178 (2015). https://doi.org/10.1021/ie504114v
119. Y. Hou, X. Li, X. Zou, X. Quan, G. Chen, Photoeletrocatalytic activity of a Cu_2O-loaded self-organized highly oriented TiO_2 nanotube array electrode for 4-chlorophenol degradation. Environ. Sci. Technol. **43**(3), 858–863 (2009). https://doi.org/10.1021/es802420u
120. Y. Hou, X. Li, Q. Zhao, X. Quan, G. Chen, Electrochemical method for synthesis of a $ZnFe_2O_4/TiO_2$ composite nanotube array modified electrode with enhanced photoelectrochemical activity. Adv. Funct. Mater. **20**(13), 2165–2174 (2010). https://doi.org/10.1002/adfm.200902390
121. J. Yan, Y. Shen, R. Cao, T. Li, $CdWO_4$ nanorods: ultrafast synthesis via a PEG-1000 polymer-assisted enhanced microwave synthesis route and their photoluminescence property. Ceram. Int. **40**(6), 8081–8085 (2014). https://doi.org/10.1016/j.ceramint.2014.01.003
122. H.W. Liao, Y.F. Wang, X.M. Liu, Y.D. Li, Y.T. Qian, Hydrothermal preparation and characterization of luminescent $CdWO_4$ nanorods. Chem. Mater. **12**(10), 2819–2821 (2000). https://doi.org/10.1021/cm000096w
123. C. Zhang, D. Guo, W. Xu, C. Hu, Y. Chen, Radiative/nonradiative recombination affected by defects and electron-phone coupling in $CdWO_4$ nanorods. J. Phys. Chem. C **120**(22), 12218–12225 (2016). https://doi.org/10.1021/acs.jpcc.6b04145
124. N. Aloysius Sabu, K.P. Priyanka, S. Ganesh, T. Varghese, Modifications in the structural and optical properties of nanocrystalline $CaWO_4$ induced by 8 MeV electron beam irradiation. Radiat. Phys. Chem. **123**, 1–5 (2016). https://doi.org/10.1016/j.radphyschem.2016.02.006
125. Z. Lin, J. Li, Z. Zheng, J. Yan, P. Liu, C. Wang, G. Yang, Electronic reconstruction of α-Ag_2WO_4 nanorods for visible-light photocatalysis. ACS Nano **9**(7), 7256–7265 (2015). https://doi.org/10.1021/acsnano.5b02077

126. W. Hou, S.B. Cronin, A review of surface plasmon resonance-enhanced photocatalysis. Adv. Funct. Mater. **23**(13), 1612–1619 (2013). https://doi.org/10.1002/adfm.201202148
127. Y. Hou, F. Zuo, Q. Ma, C. Wang, L. Bartels, P. Feng, Ag_3PO_4 oxygen evolution photocatalyst employing synergistic action of Ag/AgBr nanoparticles and graphene sheets. J. Phys. Chem. C **116**(38), 20132–20139 (2012). https://doi.org/10.1021/jp303219j
128. F. Wang, R.J. Wong, J.H. Ho, Y. Jiang, R. Amal, Sensitization of Pt/TiO_2 using plasmonic Au nanoparticles for hydrogen evolution under visible-light irradiation. ACS Appl. Mater. Interfaces **9**(36), 30575–30582 (2017). https://doi.org/10.1021/acsami.7b06265
129. J. Liu, Y. Li, Z. Li, J. Ke, H. Xiao, Y. Hou, In situ growing of $Bi/Bi_2O_2CO_3$ on Bi_2WO_6 nanosheets for improved photocatalytic performance. Catal. Today **314**, 2–9 (2018). https://doi.org/10.1016/j.cattod.2017.12.001
130. X. Liu, B. Liang, M. Zhang, Y. Long, W. Li, Enhanced photocatalytic properties of alpha-$SnWO_4$ nanosheets modified by Ag nanoparticles. J. Colloid Interface Sci. **490**, 46–52 (2017). https://doi.org/10.1016/j.jcis.2016.11.029
131. Y. Yan, H. Xing, C. Han, A. Yang, Synthesis and photocatalytic activity of Ag-$CdWO_4$ nanorods. Ceram. Int. **43**(4), 3905–3909 (2017). https://doi.org/10.1016/j.ceramint.2016.11.186
132. A.K. Chakraborty, S. Ganguli, M.A. Kebede, Photocatalytic degradation of 2-propanol and phenol using Au loaded $MnWO_4$ nanorod under visible light irradiation. J. Clust. Sci. **23**(2), 437–448 (2012). https://doi.org/10.1007/s10876-012-0450-6
133. X. Zong, C. Sun, H. Yu, Z.G. Chen, Z. Xing, D. Ye, G.Q. Lu, X. Li, L. Wang, Activation of photocatalytic water oxidation on N-doped ZnO bundle-like nanoparticles under visible light. J. Phys. Chem. C **117**(10), 4937–4942 (2013). https://doi.org/10.1021/jp311729b
134. Z. Mei, B. Zhang, J. Zheng, S. Yuan, Z. Zhuo et al., Tuning Cu dopant of $Zn_{0.5}Cd_{0.5}S$ nanocrystals enables high-performance photocatalytic H_2 evolution from water splitting under visible-light irradiation. Nano Energy **26**, 405–416 (2016). https://doi.org/10.1016/j.nanoen.2016.05.051
135. A.K. Ambast, S.K. Sharma, Variation of trap depth by dopant/codopant and heating rate in $CaWO_4$ phosphors. Opt. Quant. Electron. **49**(2), 58 (2017). https://doi.org/10.1007/s11082-017-0889-7
136. Z. Liu, J. Tian, D. Zeng, C. Yu, L. Zhu, W. Huang, K. Yang, D. Li, A facile microwave-hydrothermal method to fabricate B doped $ZnWO_4$ nanorods with high crystalline and highly efficient photocatalytic activity. Mater. Res. Bull. **94**, 298–306 (2017). https://doi.org/10.1016/j.materresbull.2017.06.021
137. G. Huang, Y. Zhu, Synthesis and photoactivity enhancement of $ZnWO_4$ photocatalysts doped with chlorine. CrystEngComm **14**(23), 8076–8082 (2012). https://doi.org/10.1039/c2ce26005k
138. X. Tian, G. Jiang, Y. Chen, M. Yin, Eu^{3+}, Li^+ doped $CaWO_4$ nanorods: synthesis, emission-decay curves and effective-refractive index. Curr. Appl. Phys. **14**(12), 1612–1615 (2014). https://doi.org/10.1016/j.cap.2014.09.010
139. C.K. Choo, S. Suzuki, K. Tanaka, Photoluminescence intensity enhancement of ion-doped $CdWO_4$ thin films prepared with pulsed laser deposition. Thin Solid Films **458**(1–2), 179–185 (2004). https://doi.org/10.1016/j.tsf.2003.12.062
140. S.H. Chen, S.X. Sun, H.G. Sun, W.L. Fan, X. Zhao, X. Sun, Experimental and theoretical studies on the enhanced photocatalytic activity of $ZnWO_4$ nanorods by fluorine doping. J. Phys. Chem. C **114**(17), 7680–7699 (2010). https://doi.org/10.1021/jp911952v
141. Y. Su, L. Hou, C. Du, L. Peng, K. Guan, X. Wang, Rapid synthesis of Zn^{2+} doped $SnWO_4$ nanowires with the aim of exploring doping effects on highly enhanced visible photocatalytic activities. RSC Adv. **2**(15), 6266–6273 (2012). https://doi.org/10.1039/c2ra20401k
142. X.C. Song, X. Cui, W.Z. Huang, Y. Zhang, H.Y. Yin, Y.F. Zheng, Photoactivity enhancement of Zn-doped $CdWO_4$ prepared with a hydrothermal method. Mater. Sci. Eng. B **197**, 31–35 (2015). https://doi.org/10.1016/j.mseb.2015.03.007
143. D. Ye, D. Li, W. Chen, Y. Shao, G. Xiao, M. Sun, X. Fu, Characterization and properties of Eu^{3+}-doped $CdWO_4$ prepared by a hydrothermal method. Res. Chem. Intermed. **35**(6–7), 675–683 (2009). https://doi.org/10.1007/s11164-009-0104-y
144. A. Phuruangrat, P. Dumrongrojthanath, T. Thongtem, S. Thongtem, Effect of Ce dopant on structure, morphology, photoabsorbance and photocatalysis of $ZnWO_4$ nanostructure. J. Ceram. Soc. Jpn. **125**(2), 62–64 (2017). https://doi.org/10.2109/jcersj2.16176
145. H. Wei, L. Wang, Z. Li, S. Ni, Q. Zhao, Synthesis and photocatalytic activity of one-dimensional CdS@TiO_2 core-shell heterostructures. Nano-Micro Lett. **3**(1), 6–11 (2011). https://doi.org/10.1007/bf03353645
146. C. Zhang, H. Hua, J. Liu, X. Han, Q. Liu, Z. Wei, C. Shao, C. Hu, Enhanced photocatalytic activity of nanoparticle-aggregated Ag-AgX (X = Cl, Br)@TiO_2 microspheres under visible light. Nano-Micro Lett. **9**(4), 49 (2017). https://doi.org/10.1007/s40820-017-0150-8
147. C. Liu, F. Wang, J. Zhang, K. Wang, Y. Qiu, Q. Liang, Z. Chen, Efficient photoelectrochemical water splitting by g-C_3N_4/TiO_2 nanotube array heterostructures. Nano-Micro Lett. **10**(2), 37 (2018). https://doi.org/10.1007/s40820-018-0192-6
148. J. Liu, Y. Li, J. Ke, Z. Wang, H. Xiao, Synergically improving light harvesting and charge transportation of TiO_2 nanobelts by deposition of MoS_2 for enhanced photocatalytic removal of Cr(VI). Catalysts **7**(12), 30 (2017). https://doi.org/10.3390/catal7010030
149. J. Liu, J. Ke, Y. Li, B. Liu, L. Wang, H. Xiao, S. Wang, Co_3O_4 quantum dots/TiO_2 nanobelt hybrids for highly efficient photocatalytic overall water splitting. Appl. Catal. B Environ. **236**, 396–403 (2018). https://doi.org/10.1016/j.apcatb.2018.05.042
150. L. Pan, S. Wang, J. Xie, L. Wang, X. Zhang, J.J. Zou, Constructing TiO_2 p-n homojunction for photoelectrochemical and photocatalytic hydrogen generation. Nano Energy **28**, 296–303 (2016). https://doi.org/10.1016/j.nanoen.2016.08.054
151. Y. Xu, Y. Huang, B. Zhang, Rational design of semiconductor-based photocatalysts for advanced photocatalytic hydrogen production: the case of cadmium chalcogenides. Inorg. Chem. Front. **3**(5), 591–615 (2016). https://doi.org/10.1039/c5qi00217f
152. S. Kment, F. Riboni, S. Pausova, L. Wang, L. Wang et al., Photoanodes based on TiO_2 and α-Fe_2O_3 for solar water splitting-superior role of 1D nanoarchitectures and of combined heterostructures. Chem. Soc. Rev. **46**(12), 3716–3769 (2017). https://doi.org/10.1039/c6cs00015k
153. P. Huo, Y. Tang, M. Zhou, J. Li, Z. Ye, C. Ma, L. Yu, Y. Yan, Fabrication of $ZnWO_4$-CdS heterostructure photocatalysts for visible light induced degradation of ciprofloxacin antibiotics. J. Ind. Eng. Chem. **37**, 340–346 (2016). https://doi.org/10.1016/j.jiec.2016.03.043
154. K. Vignesh, R. Priyanka, R. Hariharan, M. Rajarajan, A. Suganthi, Fabrication of CdS and $CuWO_4$ modified TiO_2 nanoparticles and its photocatalytic activity under visible light irradiation. J. Ind. Eng. Chem. **20**(2), 435–443 (2014). https://doi.org/10.1016/j.jiec.2013.04.038
155. X. Yan, K. Liu, W. Shi, Facile synthesis of CdS/$MnWO_4$ heterojunction with enhanced visible-light-driven photocatalytic activity and mechanism investigation. Colloids Surf. A Physicochem. Eng. Asp. **520**, 138–145 (2017). https://doi.org/10.1016/j.colsurfa.2017.01.065

156. M. Xu, T. Ye, F. Dai, J. Yang, J. Shen et al., Rationally designed n-n heterojunction with highly efficient solar hydrogen evolution. Chemsuschem **8**(7), 1218–1225 (2015). https://doi.org/10.1002/cssc.201403334
157. X. Jia, M. Tahir, L. Pan, Z.F. Huang, X. Zhang, L. Wang, J.J. Zou, Direct Z-scheme composite of CdS and oxygen-defected CdWO4: an efficient visible-light-driven photocatalyst for hydrogen evolution. Appl. Catal. B: Environ. **198**, 154–161 (2016). https://doi.org/10.1016/j.apcatb.2016.05.046
158. L. Wang, W. Wang, In situ synthesis of CdS modified $CdWO_4$ nanorods and their application in photocatalytic H_2 evolution. CrystEngComm **14**(9), 3315–3320 (2012). https://doi.org/10.1039/c2ce06656d
159. S. Bera, S.B. Rawal, H.J. Kim, W.I. Lee, Novel coupled structures of $FeWO_4/TiO_2$ and $FeWO_4/TiO_2$/CdS designed for highly efficient visible-light photocatalysis. ACS Appl. Mater. Interfaces **6**(12), 9654–9663 (2014). https://doi.org/10.1021/am502079x
160. A. Habibi-Yangjeh, M. Shekofteh-Gohari, Novel magnetic Fe_3O_4/ZnO/$NiWO_4$ nanocomposites: enhanced visible-light photocatalytic performance through p-n heterojunctions. Sep. Purif. Technol. **184**, 334–346 (2017). https://doi.org/10.1016/j.seppur.2017.05.007
161. M.S. Hassan, T. Amna, S.S. Al-Deyab, H.C. Kim, M.S. Khil, Monodispersed 3D $MnWO_4$-TiO_2 composite nanoflowers photocatalysts for environmental remediation. Curr. Appl. Phys. **15**(6), 753–758 (2015). https://doi.org/10.1016/j.cap.2015.03.022
162. Y.N. Jiang, B.D. Liu, W.J. Yang, B. Yang, X.Y. Liu, X.L. Zhang, M.A. Mohsin, X. Jiang, New strategy for the in situ synthesis of single-crystalline $MnWO_4/TiO_2$ photocatalysts for efficient and cyclic photodegradation of organic pollutants. CrystEngComm **18**(10), 1832–1841 (2016). https://doi.org/10.1039/c5ce02445e
163. K. Buvaneswari, R. Karthiga, B. Kavitha, M. Rajarajan, A. Suganthi, Effect of $FeWO_4$ doping on the photocatalytic activity of ZnO under visible light irradiation. Appl. Surf. Sci. **356**, 333–340 (2015). https://doi.org/10.1016/j.apsusc.2015.08.060
164. T. Mavric, M. Valant, M. Forster, A.J. Cowan, U. Lavrencic, S. Emin, Design of a highly photocatalytically active ZnO/$CuWO_4$ nanocomposite. J. Colloid Interf. Sci. **483**, 93–101 (2016). https://doi.org/10.1016/j.jcis.2016.08.019
165. H. Wang, C. Wang, X. Cui, L. Qin, R. Ding, L. Wang, Z. Liu, Z. Zheng, B. Lv, Design and facile one-step synthesis of $FeWO_4$/Fe_2O_3 di-modified WO_3 with super high photocatalytic activity toward degradation of quasi-phenothiazine dyes. Appl. Catal. B Environ. **221**, 169–178 (2018). https://doi.org/10.1016/j.apcatb.2017.09.011
166. T.H. Kim, C.H. Kwak, J.H. Lee, NiO/$NiWO_4$ composite yolk-shell spheres with nanoscale NiO outer layer for ultrasensitive and selective detection of subppm-level p-xylene. ACS Appl. Mater. Interfaces **9**(37), 32034–32043 (2017). https://doi.org/10.1021/acsami.7b10294
167. K. Ding, X. Zhang, J. Li, P. Yang, X. Cheng, Formation of dandelion-like $Co_3O_4/CoWO_4$ heterojunctions for enhanced supercapacitive performance. ChemElectroChem **4**(11), 3011–3017 (2017). https://doi.org/10.1002/celc.201700704
168. B. Polyakov, A. Kuzmin, S. Vlassov, E. Butanovs, J. Zideluns, J. Butikova, R. Kalendarev, M. Zubkins, A comparative study of heterostructured CuO/$CuWO_4$ nanowires and thin films. J. Cryst. Growth **480**, 78–84 (2017). https://doi.org/10.1016/j.jcrysgro.2017.10.011
169. X. Cao, Y. Chen, S. Jiao, Z. Fang, M. Xu, X. Liu, L. Li, G. Pang, S. Feng, Magnetic photocatalysts with a p-n junction: Fe_3O_4 nanoparticle and $FeWO_4$ nanowire heterostructures. Nanoscale **6**(21), 12366–12370 (2014). https://doi.org/10.1039/c4nr03729d
170. S. Yao, M. Zhang, J. Di, Z. Wang, Y. Long, W. Li, Preparation of α-$SnWO_4/SnO_2$ heterostructure with enhanced visible-light-driven photocatalytic activity. Appl. Surf. Sci. **357**, 1528–1535 (2015). https://doi.org/10.1016/j.apsusc.2015.10.012
171. G.Q. Shao, J.K. Guo, J.R. Xie, X.L. Duan, B.L. Wu, R.Z. Yuan, The Preparation of $CoWO_4/WO_3$ nanocomposite powder. J. Wuhan Univ. Technol. **19**(2), 1–3 (2004)
172. H. Zhang, W. Tian, Y. Li, H. Sun, M.O. Tadé, S. Wang, Heterostructured WO_3@$CoWO_4$ bilayer nanosheets for enhanced visible-light photo, electro and photoelectro-chemical oxidation of water. J. Mater. Chem. A **6**(15), 6265–6272 (2018). https://doi.org/10.1039/c8ta00555a
173. T.H. Do, C. Van Nguyen, K.A. Tsai, L.T. Quynh, J.W. Chen et al., Superior photoelectrochemical activity of self-assembled $NiWO_4$-WO_3 heteroepitaxy. Nano Energy **23**, 153–160 (2016). https://doi.org/10.1016/j.nanoen.2016.03.021
174. S.F. Anis, B.S. Lalia, G. Palmisano, R. Hashaikeh, Photoelectrochemical activity of electrospun $WO_3/NiWO_4$ nanofibers under visible light irradiation. J. Mater. Sci. **53**(3), 2208–2220 (2017). https://doi.org/10.1007/s10853-017-1633-1
175. J.E. Yourey, J.B. Kurtz, B.M. Bartlett, Water oxidation on a $CuWO_4$-WO_3 composite electrode in the presence of $[Fe(CN)_6]^{3-}$: toward solar Z-scheme water splitting at zero bias. J. Phys. Chem. C **116**(4), 3200–3205 (2012). https://doi.org/10.1021/jp211409x
176. F. Zhan, J. Li, W. Li, Y. Liu, R. Xie, Y. Yang, Y. Li, Q. Chen, In situ formation of $CuWO_4/WO_3$ heterojunction plates array films with enhanced photoelectrochemical properties. Int. J. Hydrog. Energy **40**(20), 6512–6520 (2015). https://doi.org/10.1016/j.ijhydene.2015.03.131
177. I. Aslam, C. Cao, M. Tanveer, M.H. Farooq, W.S. Khan, M. Tahir, F. Idrees, S. Khalid, A novel Z-scheme $WO_3/CdWO_4$ photocatalyst with enhanced visible-light photocatalytic activity for the degradation of organic pollutants. RSC Adv. **5**(8), 6019–6026 (2015). https://doi.org/10.1039/c4ra15847d
178. Y. Hou, Z. Wen, S. Cui, S. Ci, S. Mao, J. Chen, An advanced nitrogen-doped graphene/cobalt-embedded porous carbon polyhedron hybrid for efficient catalysis of oxygen reduction and water splitting. Adv. Funct. Mater. **25**(6), 872–882 (2014). https://doi.org/10.1002/adfm.201403657
179. Y. Qin, M. Long, B. Tan, B. Zhou, RhB adsorption performance of magnetic adsorbent Fe_3O_4/rGO composite and its regeneration through a Fenton-like reaction. Nano-Micro Lett. **6**(2), 125–135 (2014). https://doi.org/10.1007/bf03353776
180. P. Russo, A. Hu, G. Compagnini, Synthesis, properties and potential applications of porous graphene: a review. Nano-Micro Lett. **5**(4), 260–273 (2013). https://doi.org/10.1007/bf03353757
181. A. Wang, C. Wang, L. Fu, W. Wong-Ng, Y. Lan, Recent advances of graphitic carbon nitride-based structures and applications in catalyst, sensing, imaging, and LEDs. Nano-Micro Lett. **9**(4), 47 (2017). https://doi.org/10.1007/s40820-017-0148-2
182. L. Pan, T. Muhammad, L. Ma, Z.F. Huang, S. Wang, L. Wang, J.J. Zou, X. Zhang, MOF-derived C-doped ZnO prepared via a two-step calcination for efficient photocatalysis. Appl. Catal. B Environ. **189**, 181–191 (2016). https://doi.org/10.1016/j.apcatb.2016.02.066
183. J. Liu, J. Ke, D. Li, H. Sun, P. Liang et al., Oxygen vacancies in shape controlled Cu_2O/reduced graphene oxide/In_2O_3 hybrid for promoted photocatalytic water oxidation and degradation of environmental pollutants. ACS Appl. Mater. Interfaces **9**(13), 11678–11688 (2017). https://doi.org/10.1021/acsami.7b01605
184. A.K. Singh, K. Mathew, H.L. Zhuang, R.G. Hennig, Computational screening of 2D materials for photocatalysis. J Phys. Chem. Lett. **6**(6), 1087–1098 (2015). https://doi.org/10.1021/jz502646d

185. G. Zhang, Z.A. Lan, X. Wang, Surface engineering of graphitic carbon nitride polymers with cocatalysts for photocatalytic overall water splitting. Chem. Sci. **8**(8), 5261–5274 (2017). https://doi.org/10.1039/c7sc01747b
186. Y. Hou, M. Qiu, T. Zhang, J. Ma, S. Liu, X. Zhuang, C. Yuan, X. Feng, Efficient electrochemical and photoelectrochemical water splitting by a 3D nanostructured carbon supported on flexible exfoliated graphene foil. Adv. Mater. **29**(3), 1604480 (2017). https://doi.org/10.1002/adma.201604480
187. J. Ke, X. Duan, S. Luo, H. Zhang, H. Sun, J. Liu, M. Tade, S. Wang, UV-assisted construction of 3D hierarchical rGO/Bi_2MoO_6 composites for enhanced photocatalytic water oxidation. Chem. Eng. J. **313**, 1447–1453 (2017). https://doi.org/10.1016/j.cej.2016.11.048
188. N. Gaillard, Y. Chang, A. DeAngelis, S. Higgins, A. Braun, A nanocomposite photoelectrode made of 2.2 eV band gap copper tungstate ($CuWO_4$) and multi-wall carbon nanotubes for solar-assisted water splitting. Int. J. Hydrog. Energy **38**(8), 3166–3176 (2013). https://doi.org/10.1016/j.ijhydene.2012.12.104
189. P. Wadhwa, S. Kumar, T.J. Dhilip Kumar, A. Shukla, R. Kumar, Effect of edge defects on band structure of zigzag graphene nanoribbons. J. Appl. Phys. **123**(16), 161416 (2018). https://doi.org/10.1063/1.5011310
190. Z.B. Liu, X. Zhao, X.L. Zhang, X.Q. Yan, Y.P. Wu, Y.S. Chen, J.G. Tian, Ultrafast dynamics and nonlinear optical responses from sp^2- and sp^3-hybridized domains in graphene oxide. J. Phys. Chem. Lett. **2**(16), 1972–1977 (2011). https://doi.org/10.1021/jz2008374
191. X.J. Bai, L. Wang, Y.F. Zhu, Visible photocatalytic activity enhancement of $ZnWO_4$ by graphene hybridization. ACS Catal. **2**(12), 2769–2778 (2012). https://doi.org/10.1021/cs3005852
192. J. Xu, M. Chen, Z. Wang, Preparation of $CdWO_4$-deposited reduced graphene oxide and its enhanced photocatalytic properties. Dalton Trans. **43**(9), 3537–3544 (2014). https://doi.org/10.1039/c3dt52120f
193. J. Hao, S. Zhang, F. Ren, Z. Wang, J. Lei, X. Wang, T. Cheng, L. Li, Synthesis of TiO_2@g-C_3N_4 core-shell nanorod arrays with Z-scheme enhanced photocatalytic activity under visible light. J. Colloid Interface Sci. **508**, 419–425 (2017). https://doi.org/10.1016/j.jcis.2017.08.065
194. Y. Hou, Z. Wen, S. Cui, X. Guo, J. Chen, Constructing 2D porous graphitic C_3N_4 nanosheets/nitrogen-doped graphene/layered MoS_2 ternary nanojunction with enhanced photoelectrochemical activity. Adv. Mater. **25**(43), 6291–6297 (2013). https://doi.org/10.1002/adma.201303116
195. Y. Liu, H. Zhang, J. Ke, J. Zhang, W. Tian et al., 0D (MoS_2)/2D (g-C_3N_4) heterojunctions in Z-scheme for enhanced photocatalytic and electrochemical hydrogen evolution. Appl. Catal. B: Environ. **228**, 64–74 (2018). https://doi.org/10.1016/j.apcatb.2018.01.067
196. L. Sun, X. Zhao, C.-J. Jia, Y. Zhou, X. Cheng, P. Li, L. Liu, W. Fan, Enhanced visible-light photocatalytic activity of g-C_3N_4–$ZnWO_4$ by fabricating a heterojunction: investigation based on experimental and theoretical studies. J. Mater. Chem. A **22**(44), 23428–23438 (2012). https://doi.org/10.1039/c2jm34965e
197. N. Tian, H. Huang, Y. Zhang, Mixed-calcination synthesis of $CdWO_4$/g-C_3N_4 heterojunction with enhanced visible-light-driven photocatalytic activity. Appl. Surf. Sci. **358**, 343–349 (2015). https://doi.org/10.1016/j.apsusc.2015.07.154
198. Z.F. Huang, J. Song, X. Wang, L. Pan, K. Li, X. Zhang, L. Wang, J.J. Zou, Switching charge transfer of C_3N_4/$W_{18}O_{49}$ from type-II to Z-scheme by interfacial band bending for highly efficient photocatalytic hydrogen evolution. Nano Energy **40**, 308–316 (2017). https://doi.org/10.1016/j.nanoen.2017.08.032
199. L. Pan, J. Zhang, X. Jia, Y.H. Ma, X. Zhang, L. Wang, J.J. Zou, Highly efficient Z-scheme WO_{3-x} quantum dots/TiO_2 for photocatalytic hydrogen generation. Chin. J. Catal. **38**(2), 253–259 (2017). https://doi.org/10.1016/s1872-2067(16)62576-7
200. B. Zhu, P. Xia, Y. Li, W. Ho, J. Yu, Fabrication and photocatalytic activity enhanced mechanism of direct Z-scheme g-C_3N_4/Ag_2WO_4 photocatalyst. Appl. Surf. Sci. **391**, 175–183 (2017). https://doi.org/10.1016/j.apsusc.2016.07.104